Phys Chem Minerals (1984) 11:17–36

PHYSICS AND CHEMISTRY OF MINERALS

Some Mineralogical Applications of Synchrotron Radiation*

G. Calas[1]**, W.A. Bassett[2], J. Petiau[1]**, M. Steinberg[3]**, D. Tchoubar[4]**, A. Zarka[1]**

[1] Laboratoire de Minéralogie-Cristallographie, Universités de Paris 6 et 7, LA CNRS 09, 75230 Paris CÉDEX 05, France
[2] Department of Geological Sciences, Cornell University, Ithaca NY 14853, USA
[3] Laboratoire de Géochimie des roches sédimentaires, ERA CNRS 765, Université Paris-Sud, 91405 Orsay CÉDEX, France
[4] Laboratoire de Cristallographie, ERA CNRS 841, Université d'Orléans, 45046 Orleans CÉDEX, France

Table of Contents

Abstract. Synchrotron radiation offers several advantages over the conventional X-ray sources, among which the most important are its high intensity, broad spectral range and natural collimation. Among the numerous techniques which have been recently developed we present a review of the results concerning more specifically mineralogical systems: X-ray absorption spectroscopy concerning high-resolution edge spectra and *Extended X-ray absorption fine structure* (EXAFS), X-ray diffraction under high P-high T conditions, small-angle scattering, X-ray microanalysis and X-ray topography.

For each technique the basic principles are described together with the experimental devices used, before mineralogical examples are given. Two main applications may be pointed out: chemical and structural characterization of disordered systems and kinetic studies (phase transitions and evolution). Many other techniques (photoelectron spectroscopy, X-ray fluorescence analysis ...) which are actually under development as a result of the rapid increase of the use of storage rings are not covered in the present review but will possibly also be used in the near future in Earth Sciences.

Introduction

Synchrotron radiation is rapidly increasing as a major X-ray source in many fields. It gives quasi-parallel beams characterized by their high intensity distributed over a wide continuous spectrum of energies. These properties allow various types of experiments which could have been realized with difficulty or not at all by using X-ray tubes. After giving the fundamental properties of synchrotron radiation we will review the various types of experiments so far realized in Mineralogy (X-ray absorption spectroscopy, X-ray diffraction, small angle scattering, X-ray topography and microradiography).

* Text of an invited conference at the 13th IMA Meeting, Varna (Bulgaria)
** L.U.R.E., CNRS, Orsay, France

Some important topics have been excluded (photoelectron spectroscopies and diffraction, time-resolved spectroscopies, single crystal diffractometry, X-ray fluorescence analysis) because they have not yet been used for the study of mineralogical systems. However it must be pointed out that the development of Synchrotron Radiation is recent and that only a limited number of applications have been made on materials of mineralogical interest. We will then limit our review to the studies published or in press which largely examplify the characteristics and possibilities of synchrotron radiation and explain its present development in Earth Sciences.

Synchrotron Radiation: Production and Properties

Emission of radiation by a charged particle when it is accelerated has been known for a long time. It is predicted by the classical electromagnetic theory and has fundamental consequences in various domains. High intensity beams are now produced by high energy particle accelerators such as synchrotrons or storage rings. The interest in the light produced by these sources is based on several properties, principally its high intensity within a broad continuous wavelength spectrum and its quasi-parallel character. Two other characteristics, the nearly linear polarization and the pulsed time structure, are not so currently used but are giving rise to an increasing interest for special applications.

Initially, over the past ten years, synchrotron radiation was considered as a by-product of high-energy physics. Now a new generation of storage rings entirely dedicated to synchrotron radiation production is appearing in many countries. In fact, on account of their higher stability and of the smaller size of the source, storage rings are now definitely preferred to synchrotrons for the radiation production.

1. Characteristics of Synchrotron Radiation

The synchrotron radiation properties were recently reviewed by several authors (Kunz 1979; Winick 1980; Will 1981).

1.1. Light Emitted by an Accelerated Particle. The energy lost per turn by a particle in circular motion is given by equation (1), in the ultrarelativistic approximation (velocity of the particle $\simeq$ light velocity c)

$$\Delta E = \frac{4\Pi}{3}\frac{e^2}{R}\left(\frac{E}{mc^2}\right)^4 \qquad (1)$$

where e, E and m are the particle charge, energy and mass respectively, and R the cuvature radius of the particle trajectory. This implies that synchrotron radiation is produced efficiently by light particles such as electrons or positrons. The total intensity emitted is proportional to the ΔE value defined above for a single particle and to the intensity of the particle beam inside the accelerator. For a storage ring working at approximately 1 GeV and a few hundreds of mA, it results in a radiated power of some kilowatts which must be supplied by the radiofrequency sources. For the potential user the only problem is to recover the radiation so emitted.

1.2. Spectral Distribution. The energies of the emitted photons are distributed over a wide continuous spectrum depending on the energy of the particles and the curvature of their trajectory at the emitting point. This dependence is well characterized by a critical energy ε_C. With practical units, E being given in GeV and R in meters, ε_C is written in KeV as $\varepsilon_C = 2.218\,\frac{E^3}{R}$. Half the total power is radiated above this critical energy and half below. The general shape of the intensity spectrum is given in Figure 1 for several machines; it appears asymmetric as a result of two very different limiting forms for high and low photon energies: the intensity decreases exponentially as $\exp\left(-\frac{\varepsilon}{\varepsilon_C}\right)$ for $\varepsilon \gg \varepsilon_C$, while it decreases smoothly in a $\left(\frac{\varepsilon}{\varepsilon_C}\right)^{2/3}$ form for $\varepsilon \ll \varepsilon_C$.

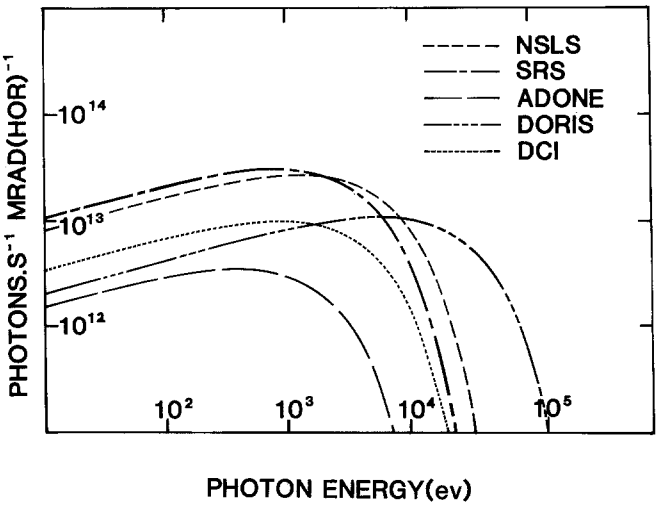

Fig. 1. Variation of the intensity emitted in a given solid angle as a function of the photon energy for various machines (see Table 1 for symbol meaning)

Two classes of machines can be distinguished according to their ε_C value:

– for soft X-ray and UV production, machines working in the 500 MeV range with R values between 0.5 and 1.5 m; the resulting ε_C is in the range 0.1–1 keV, which corresponds, in wavelengths, to the range 10–100 Å;

– for conventional X-rays, machines working in the 1 to 10 GeV range with R values between 4 and 40 meters; that gives ε_C between 1 to 10 KeV (and λ_C between 1 and 10 Å). Up to now the storage rings CESR and DORIS are the only machines providing hard X-rays by working with high ε_C values, 35 keV ($\lambda_C = 0.35$ Å) and 23 keV ($\lambda_C = 0.54$ Å) respectively.

1.3. Geometrical Characteristics. At low, classical velocity an accelerated particle is radiating in all the space directions. When its velocity is near the c limit, the emission is restricted by relativistic effects to a cone of small aperture angle (mc^2/E), centered on the direction of the particle motion (Fig. 2). For particles having a plane trajectory in an accelerator, this gives a small vertical divergence on each part of the motion plane. It is usually of the order of some tenths of m.rad. and allows the use of targets as small as 1 mm for the collimation of a high flux at distances of 10 m or more from the storage ring. In the horizontal plane

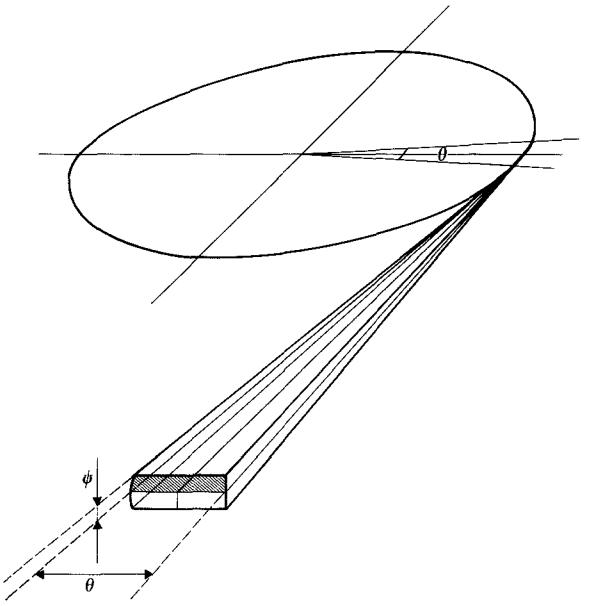

Fig. 2. Geometrical characteristics of the radiation emitted by a particle under circular acceleration. ψ is the vertical divergence of the beam

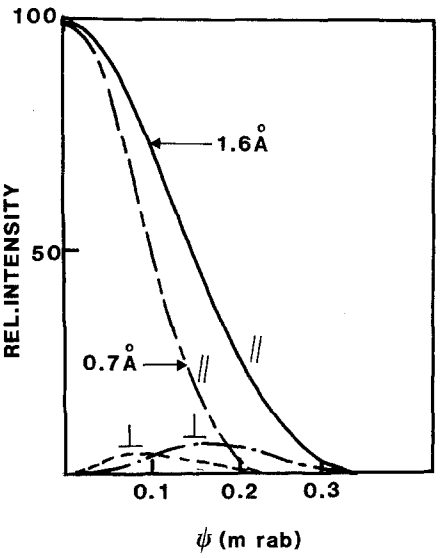

Fig. 3. Relative intensity of parallel ($N_{\bullet}$) and perpendicular ($N_{\bullet}$) components as a function of the ψ angle for the DCI storage ring working at 1.8 GeV and for various wavelengths. (From Dagneaux et al. 1975)

a nearly parallel beam can then be obtained by using the emission of a small part of the particle trajectory.

This geometrical characteristic is an important property, which favours the spectral resolution of the monochromators, but the small aperture angle implies drastic alignment conditions of the beam line and connected experiments.

1.4. Polarization. Synchrotron radiation is predominantly polarized in the horizontal motion plane of the particles. Parts of the beam emitted outside this plane are not linearly polarized: Figure 3 shows the variation of the polarization percentage as a function of angle deflection from horizontal plane depending on photon energy. In the X-ray range one can practically use 80 percent of the beam intensity having a polarization factor of 0.8. The polarization is currently taken into account in the design of the experiments (geometry of the monochromators, direction of the detectors in fluorescence analysis ...). However it has been used only recently for studying anisotropic materials. (Hahn et al. 1982).

1.5. Pulsed Time Structure. The light is produced in synchrotrons and storage rings by particle bunches of definite length (several cm to more than 10 cm) and number in the accelerator. The resulting frequency of emitted pulses is related to the radiofrequency system, with values typically of some hundred MHz. This property has found little application in the X-ray range, although it may allow, in the future, time-correlated studies of fast phenomena. (Huang et al. 1983).

2. Production of Synchrotron Radiation

About fifteen sources were in operation in 1982; they are all storage rings. High power machines entirely dedicated to synchrotron radiation production are under construction or are operational in various countries. Table 1 reports the main centers, taking into account only those used in the conventional and soft X-ray domains. The small storage rings which deliver photon beams in the UV range are not reported here because radiation in that energy range has found only limited applications in Mineralogy.

The intensity of synchrotron radiation may be compared to that emitted by X-ray tubes (Kunz 1979). However the comparison has to be made between the flux emitted through a defined solid angle which is usually very small in the synchrotron radiation case (~ 1 mrad^2). If one compares the intensity within a characteristic emission line of a powerful tube and the synchrotron radiation at disposal in the same spectral bandwidth (few eV), they are found to be of the same order of magnitude. On the other hand if a continuous spectrum is required, synchrotron radiation is much more intense than a bremstrahlung beam by four orders of magnitude. The use of new devices (wigglers, undulators) is now increasing, which allows larger intensities in a limited energy range.

In the production of X-rays at energies larger than 3–4 keV, a beryllium window is used to separate the storage ring from the beam line. This latter may be under primary vacuum because absorption is not too severe at these X-ray energies. The experiments are then made under atmospheric pressure behind a second beryllium window at the output of the beam line. In the vacuum UV and soft X-ray range, the experiments are set up under high vacuum conditions on account of the large absorption by air and because no transmitting windows are known at these low energies. The experiments are thus more difficult to carry out and no applications were made in Mineralogy apart from X-ray absorption spectra on light elements (Na, Al, Si). In most cases several beam lines are built around the same storage ring, each taking the photons emitted in an aperture of several tenth centimeters on the ring. Each beam line is used for one or more experiments that are placed at various distances (10 to 40 meters) from the ring. This provides finally to each user a photon sheet 3–5 cm wide, 1–4 mm high. According to the type of experiment this beam has

Table 1. Storage rings used as sources for synchrotron radiation in operation, 1983

Name	Location	Particle Energy [GeV]	Current [mA]	Characteristic Photon Energy [KeV]
ACO	Orsay (France)	0.55	100	0.32
NSLS (I)	Brookhaven, NY (USA)	0.70	500	0.40
ALADDIN	Stoughton, Wi (USA)	1.0	500	1.07
ADONE	Frascati (Italy)	1.5	60	1.5
SRS	Daresbury (G.B.)	2.0	500	3.2
DCI	Orsay (France)	1.8	400	3.4
VEPP III	Novosibirsk (USSR)	2.2	100	4.2
NSLS (II)	Brookhaven, NY (USA)	2.5	500	4.2
PHOTON FACTORY	Tsukuba (Japan)	2.5	500	4.2
SPEAR	Stanford, Ca (USA)	4.0	100	11.1
DORIS	Hamburg (W. Germany)	5.0	100	22.9
CHESS	Ithaca (Cornell), NY (USA)	8.0	100	35.0

to be used in its total energy range or in a narrow energy bandwidth. In this latter case it must be pointed out that the geometry of the beam (namely its quasiparallel character) makes easy the use of monochromators.

X-ray Absorption Spectra: Edge Structure

Absorption edges in the X-ray energy range are related to the excitation of core electrons from an inner shell (1 *s* for *K*-edges) to empty levels or to the continuum. This has been known for a long time by using conventional X-ray tubes, but the low intensity emitted in a continuous spectrum (Bremstrahlung) did not allow precise studies. However some important characteristics were emphasized (see the review of Srivastava and Nigam 1973). Edge studies take advantage of most of the important characteristics of synchrotron radiation: white beam character, high intensity and collimation. This allowed in recent years the recording of absorption spectra of good spectral resolution and high signal/noise ratio.

A typical absorption edge (Fig. 4) can be described as a sharp rising structure of arctangent form in the case of hydrogen-like atoms. This structure exhibits specific features in the case of atoms embedded in a compound. All the transitions responsible for these structures must obey the selection rules for electrically dipolar transitions, (e.g. $s \rightarrow p$ in the case of *K*-edges) in order to have a significant

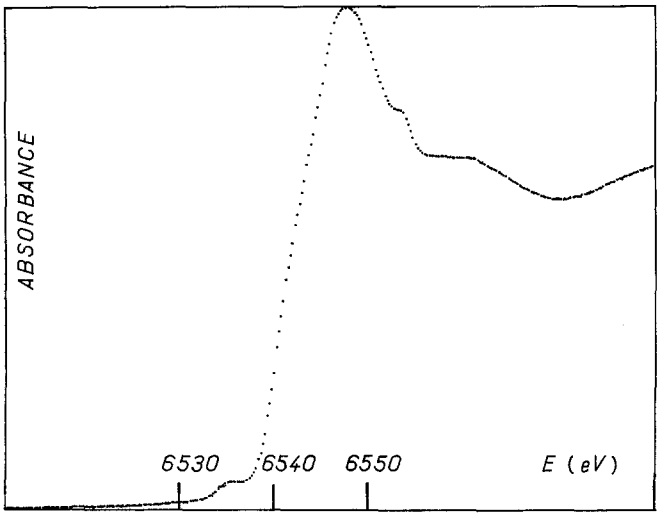

Fig. 4. Manganese *K*-edge in tephroïte (Mn_2SiO_4)

intensity. Three regions can be separated which correspond to distinct physical processes:

– For the transition elements a "prepeak" is often observed on the low-energy side of the *K*-edge. It corresponds to transitions from inner electrons to the first empty levels. They have a mainly $3d$-character in the case of transition elements of the iron family, with a $p-d$ mixing which gives the prepeak its significant intensity.

– The region between this prepeak and the absorption maximum is more difficult to interpret and extends over 15 to 20 eV before the absorption maximum, this energy range becoming larger in covalent compounds. It can be tentatively described as transitions to empty bound states which may be correlated in some compounds with molecular orbital or band structure models, depending on the type of compound. The structures in the region of the maximum of absorption are strongly dependent on the local geometry of the coordination shell. Resonance effects in the coordination cage can be observed which produce very sharp absorption maxima (or very high prepeaks).

– Beyond the maximum, the further shells must be taken into account through multiple scattering effects. This region is often referred to as X-ray Absorption Near Edge Structure (XANES) and makes a transition with the Extended X-ray Absorption Fine Structure (EXAFS) which begins 50–70 eV after the maximum and will be discussed in the following section. XANES theory is in fact not well established and its use is still limited to a few compounds (Greaves et al. 1981a; Bianconi et al. 1981).

The edge structure and its energy position give information about the oxidation state, the coordination number, the site distortion and the metal-ligand covalency. Carefully selected reference compounds have to be used for a reliable comparison, due to the lack of a priori theoretical predictions. Preliminary studies concerning Mineralogy were published by Calas et al. (1980), Petiau et al. (1981), Waychunas et al. (1983) and Calas et Petiau (1984). After a brief presentation of the experimental techniques we will discuss some potential applications of the study of X-ray absorption edges in Mineralogy, investigating successively the various crystallochemical parameters which control the edge structure and position. Among these parameters, oxidation

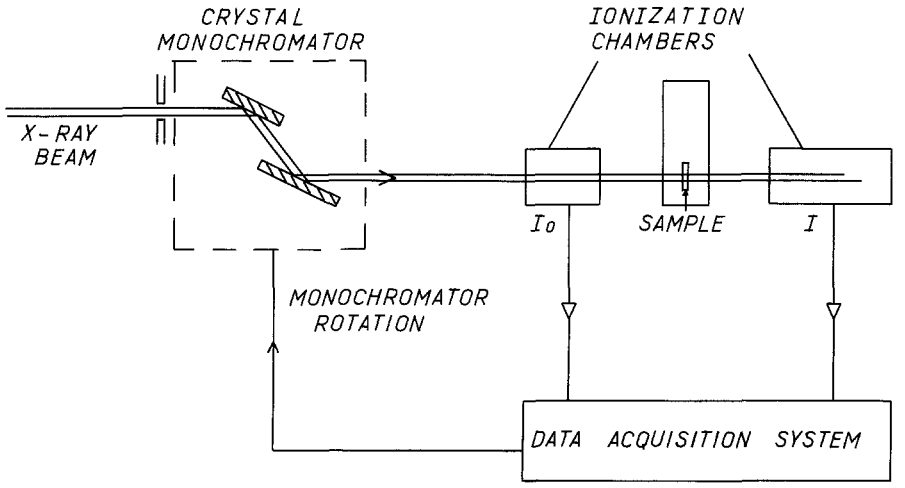

Fig. 5. Experimental setting for X-ray absorption spectroscopy

state is probably the one which has been the most extensively studied, through the well-known "chemical shift". However the spectral resolution and the large signal/noise ratio obtained with synchrotron radiation have pointed out the importance of all the other crystallochemical parameters. As a consequence the chemical shift cannot be measured independently from a careful study of the edge.

1. Experimental

Measurement of X-ray absorption spectra may be realized with different types of devices. The direct way is the transmission method which will be described below and which is in fact the only one to have been used so far in Mineralogy. Other devices replace the measurement of transmitted intensity (which gives directly the absorbance of the sample) by the detection of a physical effect which is proportional to X-ray absorption. This may be the X-ray fluorescence used for diluted systems (up to 10^{-5}), Auger electrons or photo-electron yield which are used for surface studies. The latter is the only efficient method to study light elements such as oxygen, and is also used for other elements such as aluminium. By a combination of various sources and detection techniques it is then potentially possible to study most of the elements at concentrations varying from those of main components to those of trace elements.

A typical arrangement for transmission measurements is shown in Figure 5. The white beam is monochromatized using two successive Bragg reflections, in a vertical plane for taking into account the polarization of the beam. The experimental setting is a "channel-cut" single crystal or a two-crystal device. This latter allows the elimination of reflections of higher order in the emerging beam. A good spectral resolution is necessary in order to separate the various edge features. This resolution is limited by the geometrical conditions and by the intrinsic width of the reflection curve; it can be improved by using a large Bragg angle and a beam as parallel as possible. At the Fe-*K* edge (7.115 eV), the energy spread, defined as the full width at height maximum (FWHM) of the monochromatic beam is usually 1 eV (using a Si 400 reflection). Due to the intrinsic width of the inner *K*-level (FWHM $\simeq$1.1 eV), the effective overall resolution which can be achieved is 1.3 eV. The stability of synchrotron emission allows the study of 0.1–0.2 eV shifts, and may be controlled by using reference compounds in alternance with the studied samples.

The emerging monochromatic beam goes through a first ionization chamber which gives its intensity (I_0). The sample is put beyond this first chamber and the transmitted intensity (I_1) is measured with a second ionization chamber. A computer is used to store for each energy value the corresponding intensities after voltage-frequency conversion and counting; it is also used to monitor the monochromator rotation. The energy scale is calibrated with reference compounds (often a metallic foil of known thickness). A typical absorbance spectrum $\mu(E)=\log\frac{I_0}{I_1}$ is thus obtained as a function of photon energy. An alternative possibility to this point-by-point mode is the energy-dispersive method which allows recording the whole spectrum simultaneously to study transient phenomena (Phizackerley et al. 1983).

2. Influence of Local Geometry

2.1. Coordination Number. a) The Prepeak Region. On high resolution spectra the prepeak presents a splitting of about 1.3–1.7 eV as can be observed on both Fe(II) and Fe(III) *K*-edges (Fig. 6). The transition from octahedral to tetrahedral symmetry is marked by an increase of the prepeak intensity, as can be noted in Figure 6 for Fe(II)-containing minerals. It can be interpreted as resulting from a larger $d-p$-mixing favoured by the absence of an inversion center in the tetrahedral symmetry. In the case of Fe(III) compounds this effect is even more marked owing to the closeness of the two prepeak components (Calas and Petiau 1983 b). The enhancement of the prepeak was used to show the tetrahedral symmetry of Fe(III) in some silicate glasses, and the coordination change of Ni and Co in borate glasses as a function of their alkalinity (Petiau and Calas 1983).

b) The Main Part of the Edge. For a given oxidation state and with the same ligands, the coordination number has a pronounced influence on the main edge fine structure. In Figure 7, a marked difference may be noted between 8-fold Fe(II) in almandine garnet whose *K*-edge does not exhibit any significant feature on a sharp rising slope and tetrahedral Fe(II) in staurolite whose edge is characterized by two well-marked features between the prepeak and the absorption maximum. It is to be pointed out that planar 4-fold Fe(II) gives edge structure quite different from the tetrahedral case, as shown in gillepsite (Petiau et al. 1981; Waychunas et al. 1983).

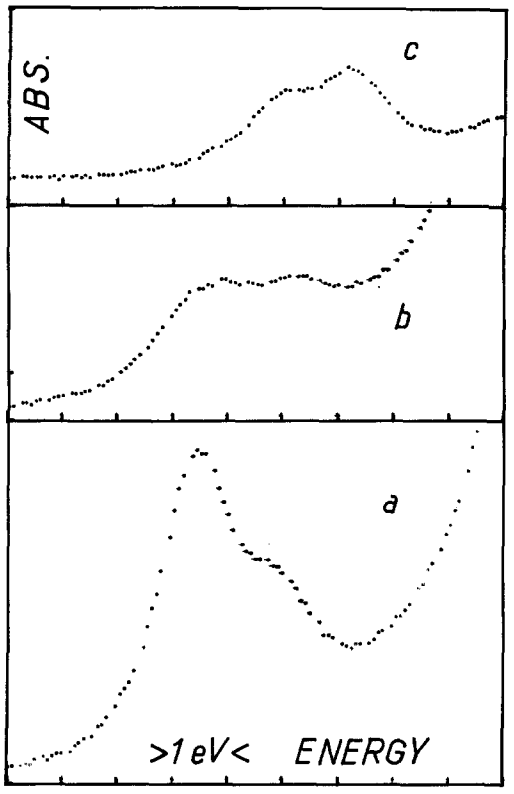

Fig. 6. Splitting of the prepeak in iron compounds. The intensity is normalized to the tenth of the absolute absorption maximum. (a) staurolite; (b) fayalite; (c) acmite

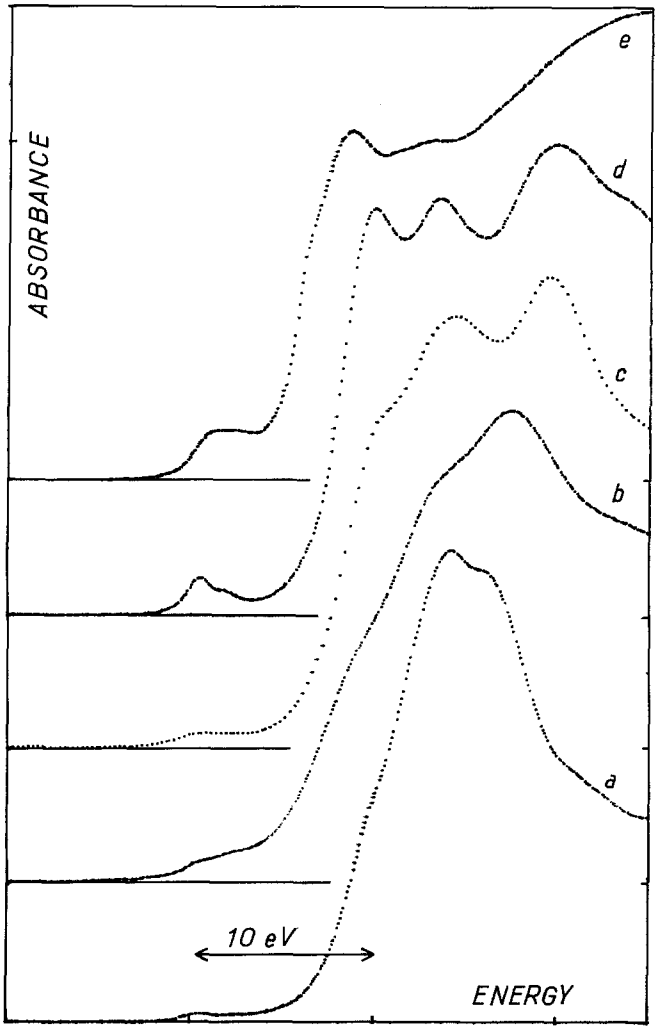

Fig. 7. Iron K-edge in various minerals. (a) almandine; (b) "FeO"; (c) hypersthène; (d) staurolite; (e) pyrite

The origin of these features is not yet firmly established as whether or not they can be interpreted by a localized model, by using molecular orbital theory. If one considers the final state symmetry it must be pointed out that the intensity of the involved transitions is related to their amount of *p* character. The characteristic features observed on tetrahedral Fe(II) edge are favoured by the absence of inversion center, as is the prepeak enhancement. Similar effects were noted for Fe(III) (Lenglet et al. 1983; Waychunas et al. 1983) and for transition elements in spinels (Calas and Petiau 1984) and this shape can thus be considered as a good indication of tetrahedral symmetry.

2.2. Distortion Effects. Distortion strongly affects the absorption maximum shape. Figure 7c gives the Fe *K*-edge of a low-Fe containing orthopyroxene (19.7% FeO), which shows a marked splitting of the maximum without any other difference with the regular 6-fold Fe(II) edges (Fig. 7a). The absorption maximum can be related to transitions to p-states of higher energy and is strongly dependent upon site geometry. No quantitative explanation was given for this effect already noted by Cotton and Hanson (1956) on Cu and Zn compounds. They tentatively suggested the action of low-symmetry crystal field, splitting the final *p*-states. As for the main edge, although not explained, these features can be used as an indication of strongly distorted sites (Calas and Petiau 1984).

2.3. Metal-ligand Distances. As can be seen in Figure 7 the absorption maximum shifts to greater energies for lower coordination numbers and hence shorter metal-oxygen distances. This was studied by Waychunas et al. (1983) who have shown that this evolution is restricted to ferrous compounds and inverse to that known in ferric and calcium compounds. These data are confirmed by those of Lenglet et al. (1983) who confirmed in spinels a positive shift of 2 eV when going from 4-fold to 6-fold Fe(III). However the data concerning model compounds where metal-ligand distances are not too widely distributed are too scarce to know if – for a given oxidation state – the absolute position of the maximum can be related with some confidence to the metal-ligand distances.

3. Influence of Chemical Factors

3.1. Metal-ligand Covalency. K-absorption edges are strongly dependent upon metal-ligand covalency. In Figure 7 two compounds having similar atomic structures are compared, Fe_xO ($x=0.92$) and pyrite. Both spectra exhibit a significant broadening of their features, perhaps in relation with the "solid-state effects" reported by Belli et al. (1980) on manganese oxides. The data concerning such concentrated and rather covalent compounds must be interpretated by taking into account correlation effects through electronic band structure calculations. The pyrite Fe-*K* edge

is mainly characterized by the intensity of the prepeak and the abrupt slope of the second feature of the edge; the maximum is strongly shifted towards greater energies and the edge extends over more than 25 eV. These features can be qualitatively explained through the one-electron energy band models (Vaughan 1978). The prepeak represents transitions to e_g-type levels (t_{2g} orbitals are fully occupied in low-spin Fe(II) compounds). The sharp rising feature indicates the beginning of the conduction band, which appears to be constituted of distinct sub-bands characterized by their *p*-state density.

The large extent of the edge is a general feature of covalent systems and is correlated to the shift to higher energies when the metal-ligand distances decrease. It is well illustrated by the Cr *K*-edge of chromates (see further, Fig. 8).

3.2. Oxidation State. In absence of any detailed feature, old spectra with poor resolution were used to fix a mean position of the edge. A marked chemical shift has been noted as a function of the oxidation state, and it was consequently measured quite systematically (Srivatava and Nigam 1973). On better resolved spectra, the various features of the edge exhibit distinct positive shifts for higher oxidation numbers. This was clearly shown on Mn- and Cu-compounds by Belli et al. (1980) and Hannoyer et al. (1982) respectively. This is due to the influence of the further parameters which affect the edge structure and position, such as coordination number, covalency effects ... The comparison must be made carefully between compounds with similar structures. The most reliable edge feature is the prepeak, on account of its more localized character. However its shift is very small, 1 eV or smaller for successive oxidation numbers, which is near the limit of reproducibility of the experiments. This discussion points out the limited accuracy and restricted usefulness of old, low resolution data based on the use of conventional X-ray sources. Indeed more detailed studies are needed in order to clear up the respective roles of the oxidation state and of the other crystallochemical parameters.

In the case of amorphous media, it is however possible to estimate oxidation states by studying main edge position: the structure of these latter are smooth and a simple translation of the edge is actually observed as a function of the oxidation state. Petiau et al. (1981) have correlated this shift to the Fe(II)/Fe(III) ratio in natural and synthetic glasses, although with a limited accuracy.

Another parameter which seems to be reliably connected with oxidation numbers is the appearance of "shape resonances" in the pre-peak region, as can be observed in some covalent complexes corresponding to extreme oxidation states, such as manganates, chromates, vanadates ... (Kutzler et al. 1980). The high intensity of these peaks is due to the very strong mixing between metal-3*d* and oxygen-2*p* orbitals. The strong internal covalent bonds make them extremely insensitive to the surrounding and they retain always characteristic shape in crystals and glasses (Petiau and Calas 1983).

We used the characteristic shape resonance of chromate edges to determine the possible presence of Cr(VI) in chlorites, where it was suspected by Besnus et al. (1975) using ESCA. Figure 8 represents Cr *K*-edges in various compounds. Chromate complexes are characterized by their shape resonant absorption as well as an absorption maximum shifted to higher energies as compared to Cr_2O_3. It

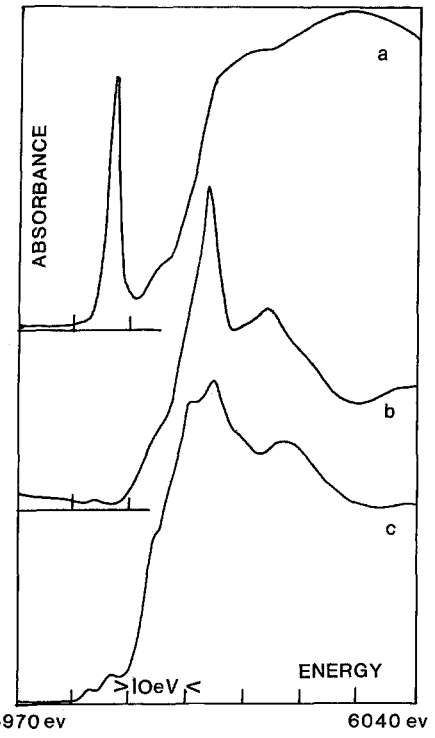

Fig. 8. Chromium K-edge in various compounds: (a) sodium chromate; (b) kammererite; (c) Cr_2O_3

can be clearly seen that the prepeak of the Cr *K*-edge in kammererite is very similar to that of Cr_2O_3: it traduces the absence of resonant shape absorption in the preedge region and then the absence of significant amounts of chromate complexes in this mineral. A similar application was published by Bianconi et al. (1982) to obtain vanadium oxidation states in glasses by using the shape resonance intensity.

X-ray Absorption Spectra: EXAFS

The decreasing absorption exhibits a modulation above the edge in all the polyatomic systems (solids, liquids and gases except the noble gases). This modulation is named the *Extended X-ray Absorption Fine Structure* (EXAFS) and extends over several hundred eV. This explains why synchrotron radiation has renewed interest in it: high intensity white beams are necessary to obtain low noise spectra, the spectral resolution being less critical than for edge studies. EXAFS carries information about the local order around a particular element. It is a method of choice to investigate amorphous or disordered compounds and its atomic selectivity allows the study of multicomponent systems.

1. EXAFS Theory

EXAFS can primarily be described as an interference effect between the electronic wave emerging from the absorbing atom and the wave back-scattered by surrounding atoms, once photoelectrons have been ejected by X-ray absorption. The theory of the phenomenon took its definite form ten years ago (Stern et al. 1975) with the systematic use of synchrotron radiation for these studies. The structural information which can be obtained concerns the determina-

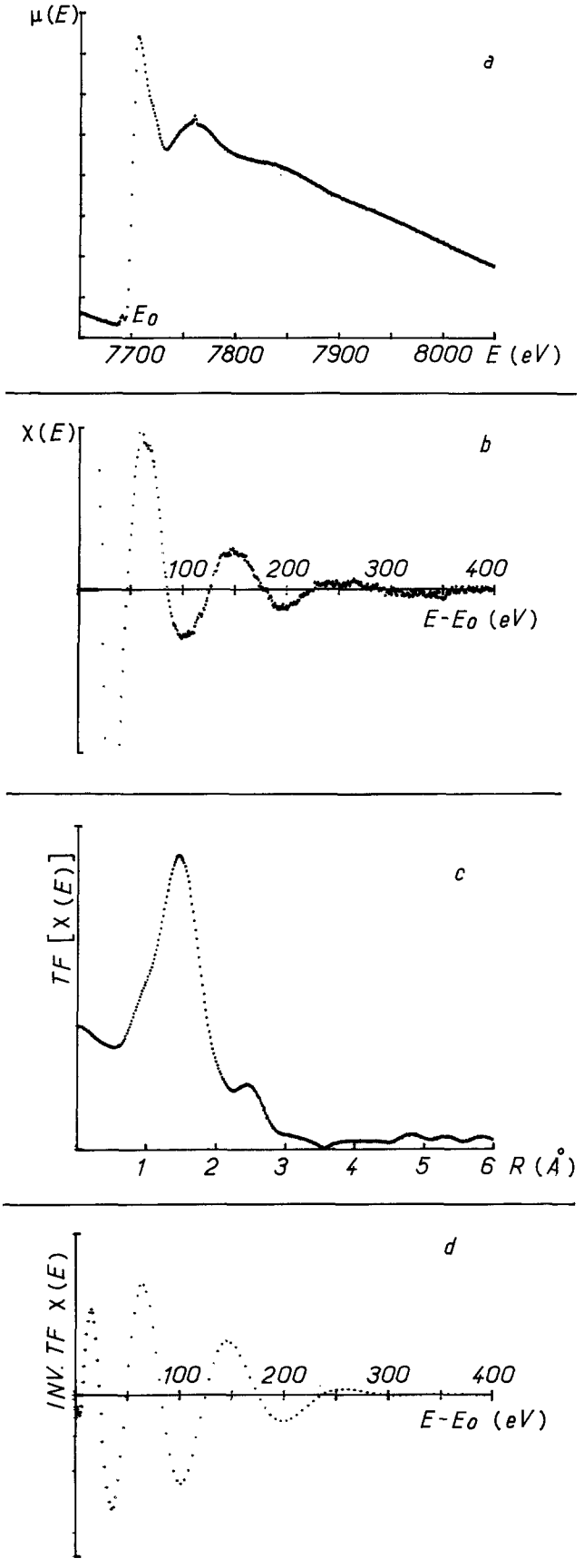

Fig. 9. EXAFS data analysis for Co(II) *K*-edge in $Na_2O-2SiO_2$ glass (4 wt% CoO). (1) experimental absorption spectrum; (b) EXAFS obtained after background substraction; (c) Fourier transform; (d) inverse transform of the first peak

tion of geometrical parameters such as interatomic distances and coordination numbers.

Some reviews appeared recently on the theoretical spects as well as on the various kinds of applications (Raoux et al. 1980; Lee et al. 1981; Hayes and Boyce 1982).

1.1. Derivation. The EXAFS spectrum is described as a sum of damped sinusoids which depend on the photoelectron wavevector k according to the relationship

$$\chi(k)=\frac{1}{k}\sum_j A_j(k)\cdot\sin(2kR_j+\phi_j(k)) \qquad (2)$$

where the index j refers to the scattering by the jth atomic shell r_j is the distance between the absorbing atom and the jth shell, $\phi_j(k)$ is a phase factor due to both central and backscattering atoms.

$A_j(k)$ is the amplitude factor defined as

$$A_j(k)=\frac{N_j}{R_j^2}|f_j(k)|\,e^{-2\sigma_j^2k^2}\,e^{-2R_{j/\lambda}}$$

where N_j is the coordination number on the jth shell, $f_j(k)$ the backscattering amplitude function corresponding to the atomic species on this shell, σ_j is the standard deviation of the R_j distances and λ the mean free path length of the photoelectron (typically 4 to 6 Å for electrons whose energy is comprised between 100 and 500 eV). These parameters allow us to discuss some EXAFS characteristics:

– The periodicity of the lattice is not inferred, so that it can be used in amorphous as well as in crystalline media.

– The various approximations used to derive the EXAFS classical theory (namely the single backscattering approach) do not allow us to use this formalism in the first 50–70 eV above the absorption edge where multiple scattering cannot be ignored (see part 2).

– The damping of the EXAFS oscillations is caused by inelastic effects responsible for the mean free path of the photoelectrons (in the range of electron energies where it is at its minimum value of several Å) and by a Debye Waller-type factor. This latter however represents only the relative fluctuation between the considered atoms and not their deviation from their respective mean position.

– The backscattering amplitude function depends on the nature of the backscatterer element. It decreases monotonously as k increases, and more rapidly for light elements such as oxygen than for heavier elements such as sulphur. For elements like 3*d*-transition atoms the amplitude has a broad maximum in the range 5–10 $Å^{-1}$. This explains why in most minerals like silicates, the contribution of the first coordination shell disappears 300 to 400 eV above the edge, the further metallic shells being observed alone above this value. This gives some limitation to the accuracy of derived metal-oxygen distances, if one takes into account the absence of EXAFS data in the first 50–70 eV.

1.2. Extraction of the Information. In order to isolate the contribution of each atomic shell, a Fourier transform of the experimental EXAFS is made after substracting the absorption background (Fig. 9). This Fourier transform in the real space (Fig. 9c) has the same significance as a partial distribution function, relative to the atomic species at whose edge EXAFS is studied, each shell contributing by a corre-

sponding peak. It is then possible to select only one shell and to obtain its contribution to the experimental EXAFS spectrum by Fourier transform of the corresponding peak (Fig. 9d). The corresponding curve is a typical damped sinusoid. By calculating the zeros of this function, obtained when $2kR+\phi(k)=n\Pi$, it is then possible to derive an experimental value of R if the function $\phi(k)$ is known. Two solutions are possible: the use of theoretical calculations of this phase shift tabulated for the various elements (Teo and Lee 1979) or the determination of the phase shift from the EXAFS data of well-known reference compounds. Both solutions imply the transferability of the phase shift.

Other parameters may also be derived from EXAFS data. The coordination number for the various shells and their chemical nature may be discussed and in favourable cases determined from amplitude analysis. Disorder effects can be studied as a function of the temperature in order to separate the thermal contribution from the static structural disorder.

2. Experimental

The same experimental device as for edge studies is used (see p. 21). Spectral resolution is however not as crucial as for edge measurements. When using "channel-cut" type monochromators, glitchs are often observed which in many cases limit the precision of the obtained data. The use of two-crystal monochromators eliminates these artefacts. In order to derive coordination numbers, special care must be taken for the sample preparation: thickness effects or sample inhomogeneities can result in wrong experimental amplitudes. Homogeneous powders deposited on scotch tape or thin sections are used, with a thickness of some tens of microns for silicates containing several percent of transition elements. High pressure studies on minerals have not advanced since the pioneering work of Ingalls et al. (1978) on pyrite compressibility.

3. Mineralogical Applications

As usefulness of EXAFS appeared ten years ago at the same time as its theoretical basis, many works were published on various kinds of compounds (glasses, solutions, crystals ...), some of which are of geochemical interest. Two kinds of applications of EXAFS were developed in Mineralogy: crystallochemistry of amorphous media (solutions, glasses, gels) and solid-solution behaviour in minerals (mainly in clay minerals). The first data were published on pyrite compressibility by Ingalls et al. (1978), on transition elements in manganese nodules (Arrhenius et al. 1979) and iron in silicate glasses (Brown et al. 1979; Calas et al. 1980).

3.1. Glasses. EXAFS makes it possible to determine interatomic distances concerning minor components of amorphous systems. The data are easier to interpret than with large angle X-ray scattering, as a consequence of EXAFS selectivity. We will summarize two types of results concerning the network-forming and network-modifying elements (for more details, see Calas and Petiau 1983a). We have chosen those concerning germanium and iron respectively because their EXAFS is easy to record in the conventional X-ray range. Main glass components such as Si, Al, Na are more difficult to study (Greaves et al. 1981b; Brown et al. 1983) and need specific devices (soft X-ray machines, detection by total electron yield, high-vacuum conditions).

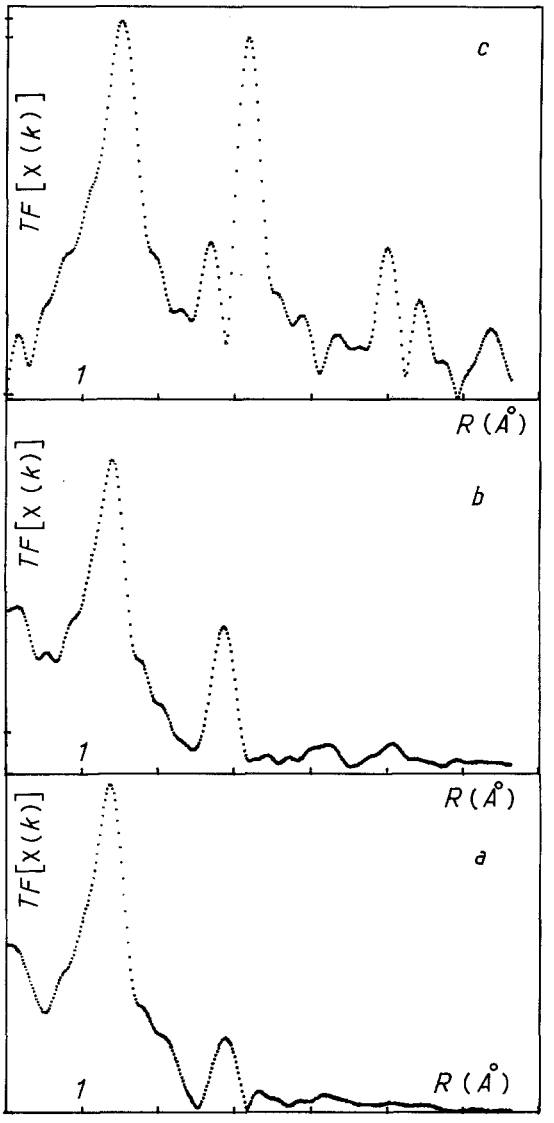

Fig. 10. Fourier transforms of Germanium K-edge EXAFS in (a) vitreous GeO_2; (b) α-quartz structure of crystalline GeO_2; (c) rutile structure of crystalline GeO_2

a) Germanium. Vitreous GeO_2 is a model compound for the vitreous silica and is one of the first to have been studied by EXAFS (Stern et al. 1975). The first peak in the Fourier transform is related to the Ge–O pair and confirms the tetrahedral coordination in glass as in a quartz type crystal (Fig. 10). The existence of a second peak is an indication of a well defined second shell (Ge–Ge pairs), due to $\widehat{Ge-O-Ge}$ angles not too widely distributed. Its position also proves the similarity with the α-quartz structure (Fig. 10b) and not with the rutile structure (Fig. 10c). The structure of some mixed glasses has been studied by Lapeyre et al. (1983). When two network-forming elements are mixed, as Ge and Si, the peak corresponding to the second shell disappears, indicating an interconnection between SiO_4 and GeO_4 tetrahedra ($\widehat{Ge-O-Ge}$ and $\widehat{Si-O-Si}$ angles are strongly different in GeO_2 and SiO_2 glasses: 130°

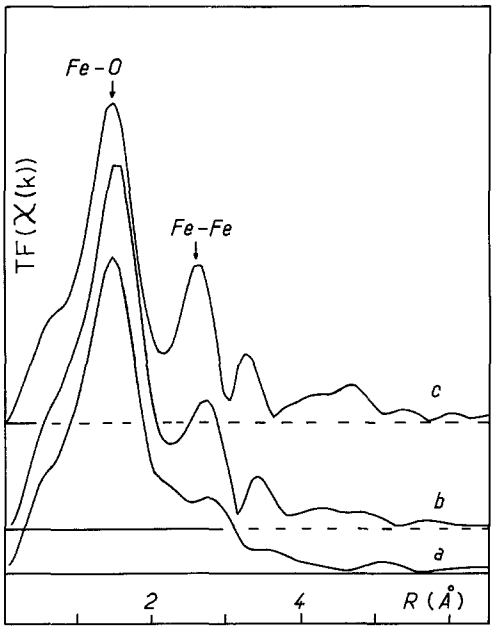

Fig. 11. Iron K-edge EXAFS during the evolution of a $Si_4Fe_2O_{11}$, nH_2O gel. (a) initital gel; (b) maturated gel; (c) reference Garfield nontronite

and 152° respectively). On the other hand the mixing with a modifying component such as sodium oxide does not affect the existence of a Ge–Ge peak at the same position as for pure vitreous GeO_2, which indicates the permanence of a three-dimensional interconnection of GeO_4 tetrahedra in the glass. The coordination change of Ge as a function of the alkali content may be followed by the Ge–O distance, which indicates a maximum of octahedral sites at about 20 percent molar Na_2O, in agreement with the other physical properties of this system and with the values obtained by Cox and McMillan (1981) on GeO_2-Li_2O.

b) Iron. Trivalent iron was found to be mainly tetrahedrally coordinated (Brown et al. 1979; Calas et al. 1980), with Fe(III)–O distances of 1.89–1.91 Å which are very similar to those encountered for tetrahedral Fe(III) in crystals. The Fourier transform (Fig. 9c) does not exhibit any significant peak beyond the first Fe–O peak. This is a fundamental difference with the Ge behaviour, indicating the absence of medium range order. Interpretation of data on divalent iron is more difficult: typical Fe(II)-O distances of 2.07 Å are found in silicate glasses which are shorter than those characterizing octahedral sites in crystals (2.15 Å typically). A similar shortening of metal-oxygen distances has been encountered for other transition metal ions in silicate glasses (Petiau and Calas 1982). This behaviour can be interpreted as resulting from a site compression in the vitreous state as compared to crystalline compounds. However a disorder effect cannot be excluded because EXAFS gives preferentially the shortest values in the case of a continuous distance distribution (Eisenberger and Brown 1979). Finally, concerning naturally occuring silicate glasses it was found (Calas and Petiau 1983a) that they follow the behaviour of synthetic glasses, with the contribution of only the first shell and intermediate Fe–O distances according to the Fe(III)/Fe(II) ratio. The absence of medium range order is very important because the presence of precipitated iron oxides has been shown by Regnard et al. (1981) in these glasses: EXAFS proves they are amorphous or at least a disordered structure.

3.2. Solutions. Interesting data were obtained on concentrated solutions, where Lagarde et al. (1980) have shown the presence of a medium range organization similar to the corresponding crystal. This points out the differences with other amorphous matrices as silicate glasses traducing distinct metal-matrix correlations. Complexation effects of nickel in solution have also been studied by Sandstrom (1982) on dilute solutions containing chlorine, which allowed him to follow the transition between hexahydrate and tetrahedral $NiCl_4^{2-}$ complex. There is no doubt that similar studies made at high temperatures will give very important data on complexation of metals in ore-forming solutions.

3.3. Silicate gels. Decarreau (1982) has studied by EXAFS at Fe *K*-edge the formation of smectites from a gel of composition $Si_4Fe_2O_{11}$, nH_2O. In Figure 11 are reported the Fourier Transforms of the initial gel (11a), of the resulting smectite as obtained by heating the gel at 150° C (11b) and of a reference Garfield nontronite (11c). The distribution curves 11b and 11c are quite similar; they exhibit a first intense Fe–O peak (measured distances of 2 Å resulting from a slightly distorted octahedral site) and two further peaks related to Fe–Fe pairs. The intensity of these latter is however smaller for the synthetic smectite than for the Garfield nontronite due to distribution effects. The most important point is the existence in the gel of Fe–Fe atomic pairs indicating a beginning of organization at a middle range scale which is similar to that of the resulting mineral. At a long range scale X-ray diffraction data have shown the absence of crystalline order. EXAFS specificity is thus pointed out as a sensitive tool to investigate the first stages of crystalline organization. Similar studies on phophate gels and apatite crystallization were published by Hasnain and Hukins (1981) who have followed the maturation of amorphous calcium phosphate using EXAFS at the Ca *K*-edge.

3.4. Clay Minerals. Iron in kaolins was studied by Bonnin et al. (1982). Iron oxide phases already detected by ESR and Mossbauer experiments were investigated by EXAFS at the Fe *K*-edge. The complementarity between these techniques allowed them to discuss the nature and average size of these phases, as well as their crystalline organization. The existence of an important disorder beyond the first coordination shell, although not detectable by Mossbauer spectroscopy, was proved by EXAFS.

Ni–Fe–Mg hydrated secondary silicates from ore deposits of New-Caledonia were studied by Manceau and Calas (1984). Fourier transform of the EXAFS of Ni in lizardite (Fig. 12) exhibits two well marked peaks: the first peak corresponds to Ni–O pair and confirms the octahedral coordination of Ni with Ni–O distances slightly reduced as compared to NiO reference; the second peak is more complex because it traduces the nickel-metal pair. With the expected distances for octahedral layer cations it is impossible to separate Fe from Ni on the second shell, because they have nearly the same amplitude and phase backscattering factors. The presence of the light element Mg is evidenced by a lower intensity of this peak in relation to its lower backscattering factors (both phase shift and amplitude). It is hoped to discuss substitution mechanisms (regu-

lar substitution, microdomains ...) by using this second peak intensity, in order to correlate them with geological formation conditions. Similar studies were made by Bonnin et al. (1984) on Mg–Fe substitution in various phyllosilicates. A good agreement with X-ray diffraction was found concerning Fe–O distances data, but the Fe-(Mg, Fe) distances were found at slightly shorter values. The peak intensity was again correlated with the Fe-content of the second shell (thus depending on the substitution ratio) and also with the tri-or di-octahedral nature of the phyllosilicate.

Energy Dispersive X-ray Diffraction

Synchrotron radiation has not yet found general application to structure determination of minerals by conventional techniques such as single crystal diffractometry or high-resolution powder diffractometry. On the contrary specific methods have received more attention, mainly energy-dispersive X-ray diffraction. Anomalous dispersion has also been used to resolve ambiguities in structures containing elements with similar atomic numbers; it has been applied to the determination of cation site occupation in spinels (Yakel 1980).

The energy dispersive method makes possible fast structure identification, particularly in studies of phase transformations at elevated temperatures and high pressures. Synchrotron radiation has proved to be particularly useful for studies made with the diamond anvil cell in which the sample is very small. The features of synchrotron radiation which make it desirable for this kind of research are:

1. the high intensity which makes it possible to collect data on a very small sample over a very short time period;

2. the smooth dependence of intensity on energy which makes it ideal for energy dispersive techniques;

3. a high collimation;

and 4) the high energies available, especially at the Cornell High Energy Synchrotron Source (CHESS), which allow the X-rays to enter and leave the pressure vessel with a minimum of absorption.

The first studies made on minerals concerned FeS compressibility up to 70 kbar and at room temperature (Buras et al. 1977; Will 1981). More recently structural modifications at phase transitions were studied in KCl and KI (Skelton et al. 1982), in fayalite (Furnish and Bassett 1983) and magnetite (Bassett, unpublished).

1. Experimental

Mechanisms of the structural changes occuring at phase transitions are studied at the Department of Geological Sciences at Cornell University by using a diamond cell with small resistance heater wound around the diamond anvils seats. A thermocouple placed in contact with one of the diamond anvils is used to measure the temperature. The apparatus is placed in a cave on one of the white beam lines of CHESS and diffraction patterns are obtained by energy dispersion using an intrinsic germanium detector (Fig. 13). The pressure is increased by remote control from outside the cave using a synchro motor and a set of worm gears to turn a screw that drives the diamond anvils together. The temperature is also controlled from outside the cave by variable transformers. Conditions up to 300 kbar and 600° C are easily and rapidly achieved.

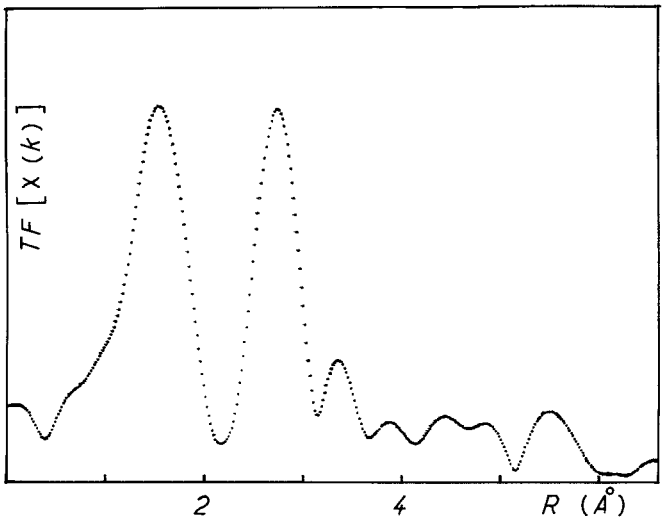

Fig. 12. Fourier transform of the Nickel *K*-edge EXAFS of Ni–Mg–Fe lizardite

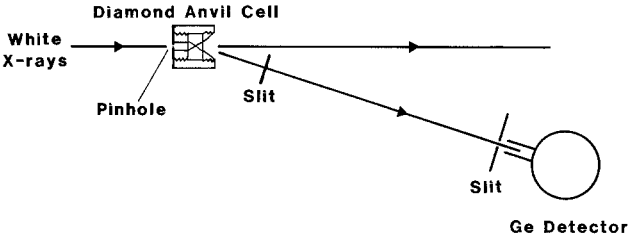

Fig. 13. Instrumentation for energy dispersion X-ray diffraction of a sample at high pressure and temperature. A white X-ray beam from the synchrotron enters the diamond anvil cell through a pinhole 100 microns in diameter, passes through the first diamond to impinge on the polycrystalline sample under pressure and at high temperature between the diamond anvils. Scattered X-rays pass through the other diamond, through the slits and enter the intrinsic germanium detector. The intensity of the scattered X-rays is then displayed on a cathode ray tube as a function of energy

2. Mineralogical Applications

2.1. Olivine-Spinel Phase Transition. It had been suggested by Poirier (1981) that olivine may undergo a martensitic type of phase transformation as the anions glide from approximately hexagonal close packed arrangement in the olivine structure to the cubic close packed arrangement in the spinel structure. Furnish and Bassett (1983) suspected that the anions might undergo the martensitic type of change, but the cations might require more time to become ordered in the spinel structure. As a consequence, there might be an intermediate stage during the transformation when the anions had undergone the rearrangement but the cations had not. This would place the anions in a cubic close packed arrangement while the cations remained in an essentially disordered arrangement. The effect of this would be to produce a cubic unit cell that is half as large as the spinel unit cell because it is the cations which establish the larger size of the spinel cell. Consequently, the intermediate stage should produce a pattern with peaks consistent with the smaller unit cell ($h/2$, $k/2$, $l/2$ all even or all odd) and the peaks consistent with only the larger unit cell should appear later (Fig. 14).

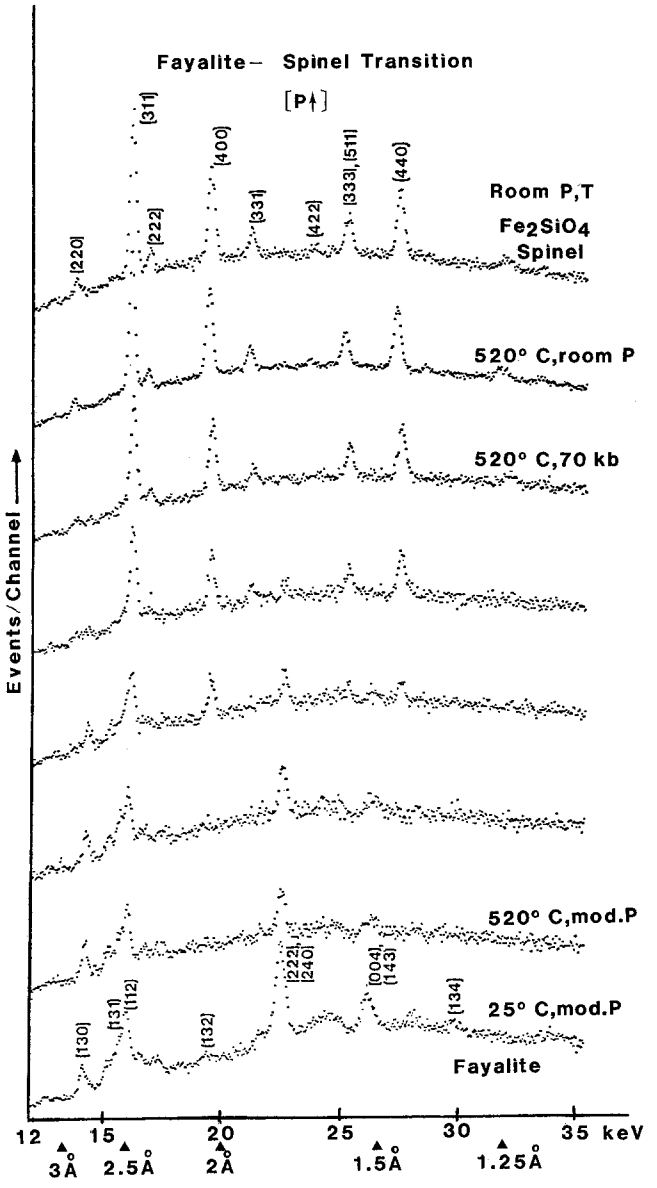

Fig. 14. Diffraction patterns of a fayalite as pressure is increased through the transition from olivine to spinel structure at 520 degrees centigrade. Note that as the transition progresses from the bottom toward the top, the 400 reflection of the spinel structure appears before the 331 reflection

At approximately 520 degrees centigrade, increasing pressure produced a transient intermediate stage having the peaks described above. At 400 degrees centigrade the intermediate stage lasted for considerably longer and could be quenched and examined by the Debye-Scherrer method which has better resolution than the energy dispersion method. The Debye-Scherrer patterns revealed additional peaks whose behavior confirmed the existence of the intermediate stage in which the anions are in a cubic close packed arrangement while the cations are not ordered in the cubic spinel arrangement.

2.2. Phase Transition of Magnetite. Another study which takes advantage of the rapid rate of data acquisition possible with synchrotron radiation is the mapping of phase boundaries. It is possible to make a rapid survey of phases present over a range of pressures and temperatures and by so doing to establish the locations and slopes of phase boundaries. With this technique it is possible to acquire a new data point every two minutes, and so a whole phase diagram can be determined in a few hours.

This technique was applied to the determination of the phase boundary separating the low pressure phase from the high-pressure phase of magnetite. A thermocouple placed in contact with one of the diamond anvils was used to measure the temperature and metallic gold was mixed with the sample as a pressure calibrant.

The results of this study are preliminary. However, it was established (Bassett, unpublished) that the boundary has a slope that lies between -2 and $-6°$ C/kbar. The transition occurs in the pressure range from 150 to 250 kbar. This phase boundary does not necessarily correspond with the equilibrium phase boundary because the transition is more sluggish at lower temperatures.

Small-Angle Scattering

The field of application of such a classical method has been considerably extended owing to the use of synchrotron radiation. The principal advantages of this latter source which are used here are its high intensity, white beam character and small vertical divergence.

1. Experimental

The small angle scattering assembly working at LURE-DCI, Orsay (France) is represented in Fig. 15. Due to the small vertical divergence of the beam (0.2 mrad) it uses a singly curved monochromator in order to focus the beam in the horizontal plane and to obtain an almost punctual image (Lemonnier et al. 1978). This device is constituted by a germanium crystal plate with variable curvature: it focuses at 2 m an image of 800 μm width and 8 mm height. A simple parallel collimation device allows the image to be reduced in height in the vertical plane to 300 μm. It

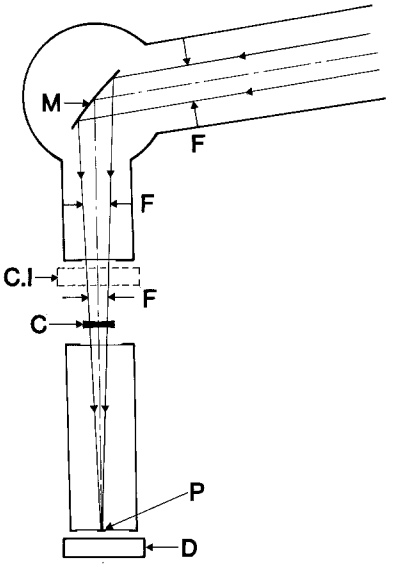

Fig. 15. Experimental assembly: F = antidiffusing slits; CI = ionization chamber; P = trap; M = monochromator; C = sample; D = detector

is thus possible to realize almost punctual collimation conditions for $S>10^{-3}$ Å^{-1} ($S=\varepsilon/\lambda$ where ε is the scattering angle and λ the wavelength of the monochromatized beam). The spectral resolution obtained $\Delta\lambda/\lambda$ is about 4.10^{-3}. Under usual run conditions at LURE-DCI (1.8 GeV and 150 mA) the total incident flux is about 10^{11} photons/s.

Small-angle scattering diagrams obtained in these conditions can be considered as free of instrumental distortions due to beam shape and spectral composition (Tchoubar et al. 1978). Data processing is then considerably simplified either when considering the direct processing by Fourier transform methods, when finding characteristic laws or when comparing experimental curves to simulated spectra.

Due to the high beam intensity the recording time of an experimental spectrum is then considerably reduced with respect to that required when using a conventional source. The reduction factor attains 200 to 500 and this allows one to watch weakly diffusing or quickly evolving systems. It is also possible to study the precise morphology of the diffusing particles and their mutual relations. With this powerful tool the way is open for a new generation of "in situ" kinetic studies as a function of various parameters.

2. *Mineralogical Applications*

2.1. Gel Formation by Swelling of Smectite in Water. The evolution of smectite-water systems, with a fixed water content, has been studied by cooling at −70° C and subsequent slow heating up to room temperature (Pons et al. 1981 and 1982). The scattering diagrams were recorded "in situ" (i.e. non destructive experiment) and are characterized by a very low noise. The experimental curves have been compared to simulated spectra. A good agreement can be obtained by considering two factors: first the position and width of the 001 peak correspond to the interlayer distance values inside the particles and to their distribution; secondly the intensity of this 001 peak and the scattering in the very low angle range give the layer content and average size of the particles.

Diagram evolution as a function of the temperature (Fig. 16) shows that the macroscopically continuous swelling process, which allows the transition from a solid clay to a thixotropic gel, actually develops through a succession of states defined at the level of the interaction between neighbouring layers. The resulting gel is characterized by parallel layers within unit stackings (homogeneous hydration domains) accompanied by a disorientation between these stackings. These results show that there exists a first-order transition corresponding to the change from attractive to repulsive mode of the electrostatic interactions. The possibility of such a system for crossing the threshold of this transition is closely connected to the charge of the layer and to the hydration energy of the cations and their chemical potential of specific adsorption.

2.2. Hydrolysis-Precipitation Process of Aluminium Hydroxide from Aqueous solution. Aluminium geochemistry is of first interest in surface geology; solubilization and precipitation processes are still greatly unknown. The first steps of hydrolysis processes have recently been studied by small-angle scattering based on synchrotron radiation by Bottero et al. (1982). Using refined models, these authors were able to define the morphology of the particles at various stages of their evolution. As the experimental spectra were not

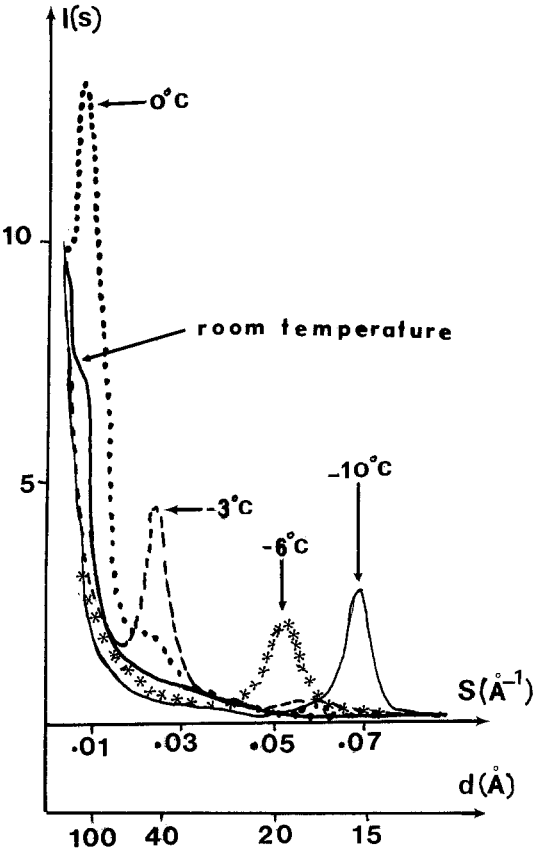

Fig. 16. Evolution of the swelling as a function of temperature (Kozakov saponite Li)

deformed, it was quite easy to observe the characteristic laws of largely dispersed colloidal particles or diluted micels (Guinier and Fournet 1955; Glatter and Kratky 1982). These laws allow the determination of some mean geometrical parameters whose significance is shortly given thereafter:

1) The mean volume V of a particle is given by $V=I(O)/P(O)$, where $I(O)$ is the value at the origin of the intensity scattered by the solution and $P(O)$ is its total scattering power.

2) The radius of giration R_g can be deduced directly from the experimental curves by using the Guinier relation for the innermost part of the scattering

$$I(S)=I(O)\exp\left(\frac{-4\Pi^2 R_g^2}{3}S^2\right) \tag{4}$$

where $I(S)$ is the scattered intensity at the scattering vector S.

Similar laws can be observed for anisotropic particles and verified in the intermediate range of scattering angles.

3) The specific surface is deduced from the Porod'law in the outermost part of the scattering

$$\lim \frac{8\Pi^2 S^4 I(S)+}{P(O)}=\frac{\langle\sigma\rangle}{\langle V_P\rangle} \tag{5}$$

where $\langle\sigma\rangle$ is the mean external surface per particle and $\langle V_P\rangle$ the mean value of the particle volume.

By comparing these various parameters, Bottero et al. (1982) have deduced a model for a mean particle evolution

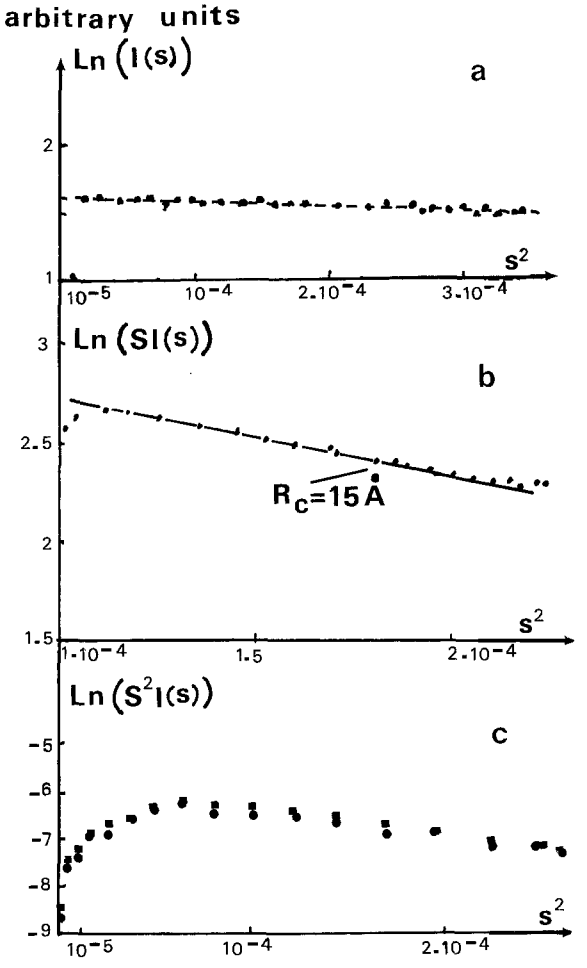

Fig. 17. (a) Scattering curve of the polymeric ion Al_{13}. (b) Characteristic experimental curve for rod-like particles in the solution $R=2.5$ aged 90′. (c) Characteristic experimental curve and simulated curve for plate like particles in the solution $R=2.5$ aged 24 h

in aqueous solutions of $AlCl_3$ 0.1 *M* partially neutralized at neutralization ratios $R=\frac{NaOH}{Al}$ equal to 2 and 2.5. The evolution is schematized in Figure 17. For the solution $R=2$, there is a linear evolution of $\ln I(S)$ against S^2 in the angular domain considered. By using the Guinier law (4) the giration radius is 9.8 Å. Previous NMR results (Bottero et al. 1980) have shown the existence of $Al_{13}O_4(OH)_{28}^{3+}$ with an icosahedral symmetry of Al atoms. The use of a spherical model gives an effective radius of 12.6 Å which confirms the hydration of the central unit. These polymers are either isolated or counterbalanced by Cl^- ions. The $R=2.5$ solution contains particles which develop very quickly with the time during the first 24 h, after the preparation. The ageing process first gives after 1.30 h cylindrical particles (300 Å long and 30 Å diameter) which can be considered as associations of the above-mentioned particles. There is a subsequent densification of these particles by the reorganization of internal bonds and release of Cl^- ions in the solution, as probably some of the elementar polymers. Afterwards these thread-like clusters are associated in the form of platelets with an average thickness of 60 Å and average diameter of 1,000 Å after 24 h ageing. These particles retain a great specific surface which explains their floculating efficiency.

By using the advantages of synchrotron radiation the small-angle scattering experiments have given the first direct structural data on the elementary stages of the formation of aluminium hydroxides: the evolution is towards the formation of an amorphous gel of pseudo-boehmite type. They explain also the role of Cl^- ions as crystallization inhibitors in these systems.

X-ray Microradiography

Most geological samples are heterogeneous. Thus, in addition to classical optical study of thin sections, several methods (electronic and ionic microprobes, scanning electron microscope coupled with EDAX systems, scanning transmission electron microscope equipped with energy loss spectrometer etc ...) have been developed during the last decades in order to study the spatial distribution of chemical elements. Because of these instruments it is now possible to analyse with considerable accuracy very small samples or to demonstrate the distribution of elements on very small scales. Although these methods are certainly very useful, in some cases, it is important to chart elements on somewhat larger scales, i.e. a few cm^2. Pedological concretions or manganese nodules, for instance, composed of fine, opaque Fe–Mn oxides, exhibit textures visible only on thin-section scale and it is impossible to obtain a comprehensive view of this texture with methods such as microprobe. This method may not be considered as competing with microanalysis techniques but, on the contrary, to define the spatial distribution of elements over relatively large fields with a resolution as accurate as possible.

For this purpose, synchrotron radiation is useful in both its very good geometrical definition and collimation, which avoids experimental distortion of the image, and its intense white beam character, which allows one to study selectively all the elements heavier than K.

1. Principle of the Method

X-ray microradiography takes advantage of the existence of X-ray absorption edges (see part 2). On both sides of the edge the marked variation of the absorption coefficient (Fig. 18) makes it an analytical method. It takes advantage

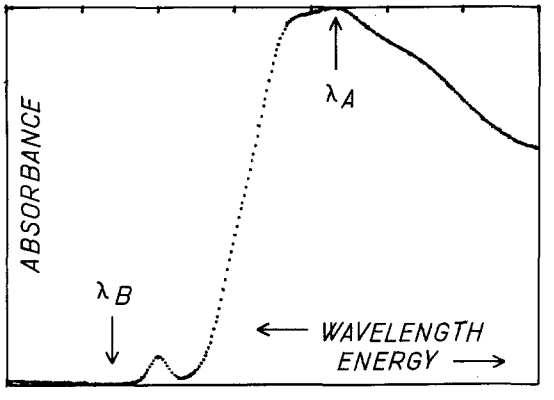

Fig. 18. Variations of the coefficient of absorption in function of the wavelength for a given element (Fe(III) *K*-edge in a silicate glass as an example)

of the selectivity of X-ray absorption spectra, allowing the study of complex compounds. The analysis may be performed by recording two contact microradiographs, the first with a wavelength corresponding to the maximum of absorption, (λ_A, Fig. 18), the second with a wavelength corresponding to the minimum (λ_B, Fig. 18). At maximum absorption, areas containing relatively high concentration of the studied element absorb more photons and appear whiter on the photographic plate; at minimum absorption, X-rays are not absorbed and the plate is darker.

This principle has been known for more than thirty years (see e.g. Cosslet and Nixon 1960) but the development of an X-ray microscope was confronted with two difficulties: (1) the too lowpower of traditional X-ray sources, (2) their too low width of spectrum. This was overcome using synchrotron radiation because its luminance is very high and, furthermore, it is a white light covering most of the X-ray energy field (Polack et al. 1978; Kirz 1980).

2. Experimental

The schematic diagram of the recording experiment is given in Figure 19 (Bigler et al. 1982). The mains units are: (1) the synchrotron radiation, (2) a tunable monochromator, (3) the detector which is a photographic plate and (4) an automatic exposure meter. The first and so far the only studies published on minerals used the synchrotron radiation delivered by the storage ring D.C.I. (LURE, Orsay, France) which presents a very small divergence. The experiment is set up at 24 m from the source and, in this condition, the area of the beam is about 8×30 mm. Thus approximately 3 cm^2 of the sample can be illuminated. A channel-cut monochromator made of silicon (220) is used which is held under vacuum and does not change the area of the beam. The monochromator being tunable it is possible to change the wavelength of the emergent beam and thus to study several chemical elements in the same sample (the use of synchrotron radiation is essential for this purpose because of its white beam character.

The sample is a thin section approximately 30 μm thick glued to a mylar foil and fixed to the detector which is a high resolution photographic plate (Kodak H.R.). During the first experiments, the images obtained (Polack et al. 1978; Steinberg et al. 1979) presented some defects appearing as horizontal white or black lines. These are related to imperfections in the silicon crystal surface of the monochromator. In order to average these defects, plate and sample are translated horizontally in a sinusoidal way during the exposure.

Because the intensity of the synchrotron radiation decreases during the course of time, an exposure meter was built (Bigler 1982; Bigler et al. 1982). It is based on a flowing gas X-ray counter which measures the radiation scattered by air (Fig. 19). An electron digital preselection counter follows, and stops the exposure when each plate has received the same number of photons. Usually exposure times are between 6 and 10 min. Thus, for each sample, and for each element studied two photographs are obtained.

The information concerning the location of the element and, eventually its concentration, can be obtained by comparing the two plates. In a first approach, the relative variation of the number of photons transmitted by a sample on both sides of an absorption edge is related to the concentration of the element through the following expression (Polack et al. 1978)

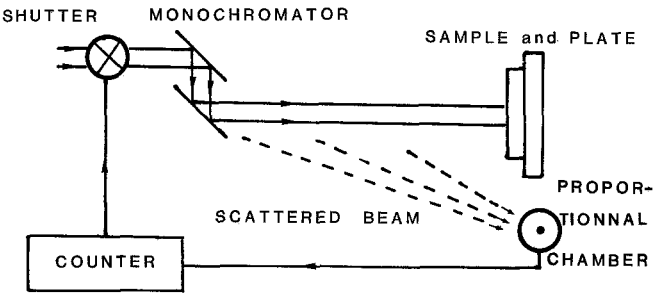

Fig. 19. Schematic diagram of the recording experiment used for X-ray microradiography

$$\Delta N/N = 1 - \exp(-\rho e \Delta \mu C). \quad (6)$$

In relation (6) $\Delta\mu$ means the variation of the absorption coefficient on either side of the absorption edge, ρ the density of the sample, e its thickness and C the concentration of the studied element.

Visual estimation of the relative darkness of photographic plates is unreliable and thus experimental images are analysed by a digital process (Bigler 1982). The images are digitized with a microdensitometer that offers a minimum aperture of 5×5 μm^2. Usually, we work with a 20×20 μm^2 aperture and record 256×256 pixel image covering 5.1×5.1 mm^2 field of the sample. Subsequently, image is digitized to 12 bits. Digital processing involves the calculation of: $\mathrm{Ln}(D_{\min}) - \mathrm{Ln}(D_{\max})$, where $D_{\min}$ = density of the image recorded at the minimum of absorption of the element and $D_{\max}$ recorded at maximum absorption. The final image resulting of this subtraction is displayed on television monitor.

3. Element Distribution in Manganese Nodules

Figure 20 illustrates portion of a manganese nodule from the Clarion-Clipperton area, N.E. Pacific Ocean. The botryoidal texture lies near the cortex of the nodule. On these illustrations, the presence of an element appears as white areas while dark denotes its absence. Nickel is clearly located in areas containing much manganese and where iron is depleted or absent. Similar results have been obtained by chemical analysis or microprobe studies but, to our knowledge, the spatial correlation between Mn and Ni (and the inverse correlation between Fe and Mn) has never been imaged on such a scale. Using the same method, we were able to compare textures in recent nodules, in nodules embedded in oceanic sediments and in fossil nodules outcropping on land (Steinberg et al. 1983).

Finally, one may evaluate this method to see if it leads to quantitative data. Theoretically, the final images show the spatial repartition of the element expressed as mass per unit area (m); the concentration can be deduce if one knows the sample density (ρ) and its thickness (e) because $C = \frac{m}{\rho \cdot e}$. If, for the illustrated sample whose thickness is 30 μm, one assumes 4 as being its average density, we obtain the results summarized on Table 2 (Bigler 1982). They are compared with data obtained on S.E.M. equipped with an EDAX system.

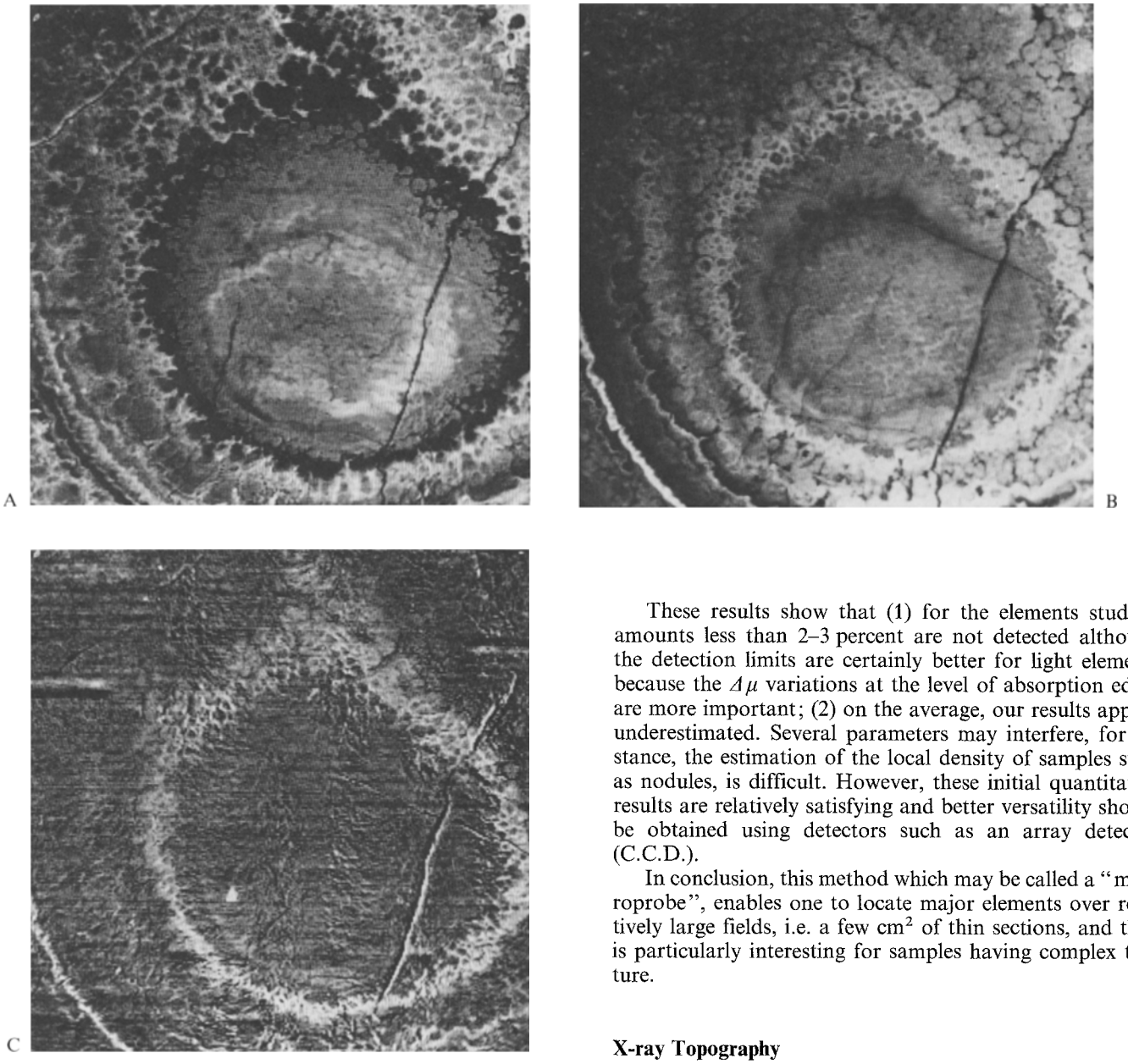

Fig. 20. Polymetallic nodule from the Clarion-Clipperton area (NE Pacific-Each image covers a 5.1×5.1 cm^2 field. The presence of an element appears as white areas while dark denotes its absence. (A) Iron (B) Manganese (C) Nickel

Table 2. Chemical analyses obtained on a manganese nodule

	Mn		Fe		Ni	
	(1)	(2)	(1)	(2)	(1)	(2)
Areas rich in Mn – Ni	28%	37%	>1.5%	1.7%	3%	3.4%
Areas rich in Fe	15%	29%	10%	16%	>1%	0.3%

(1) X-ray contact analysis near an absorption edge
(2) S.E.M. equipped with EDAX

These results show that (1) for the elements studied, amounts less than 2–3 percent are not detected although the detection limits are certainly better for light elements because the $\Delta\mu$ variations at the level of absorption edges are more important; (2) on the average, our results appear underestimated. Several parameters may interfere, for instance, the estimation of the local density of samples such as nodules, is difficult. However, these initial quantitative results are relatively satisfying and better versatility should be obtained using detectors such as an array detector (C.C.D.).

In conclusion, this method which may be called a "macroprobe", enables one to locate major elements over relatively large fields, i.e. a few cm^2 of thin sections, and thus is particularly interesting for samples having complex texture.

X-ray Topography

X-ray topography is an imaging technique which has been applied to several minerals (quartz, fluorite, topaz, beryl ...) by using conventional sources (Scandale and Zarka 1982). It is sensitive to reflecting power differences due to the strain fields generated around the defects in crystal and are mainly used for the study of dislocations, planar defects or large precipitates, with a resolution lying in the micron range. This kind of information obtained is related to the sample history (growth conditions, plastic deformation ...). The characteristics of synchrotron radiation which can lead to an improvement of topographic studies vs the use of classical generators are: the small angular spread, continuous spectral distribution, high intensity and lateral extension of the incident beam. Two types of studies can be developed with synchrotron radiation (Sauvage and Petroff 1980): white beam topography and tunable monochromatic topography. After giving the experimental characteristics of both techniques, we will give their recent application to quartz (with respect to α-β phase transition and growth

defects, respectively). Grown-in lattice defects were also recently studied in beryl (Herres and Lang 1983) and diamond (Lang et al. 1983).

1. White Beam Topography

1.1. Experimental. The crystal is immersed in the white X-ray incident beam and a number of lattice planes select out of the continuous spectrum the proper wavelength to be reflected according to the Bragg law. This property is well known (Laue method) but in this case each diffraction spot is a high resolution topograph due to the low divergence of the beam delivered by the storage ring. The possibilities of this technique have been investigated by Tuomi et al. (1974) and Hart (1975). The advantages are important:

- no great need is necessary for positioning the sample;
- there is no scanning of the sample needed;
- several diffraction spots may be simultaneously recorded;
- it is possible to record homogeneous images even with warped samples, subgrain structures or even polycrystalline materials.

However the white beam topographic technique presents the drawback that the images result in many cases from the superposition of several harmonics whose relative importance can be estimated from various parameters: emission spectrum of the source, structure factors, absorption of the beam by the beryllium window, the air and the sample, and finally by the detector response.

White beam topography corresponds to a very simple experimental setting allowing special devices such as furnaces to be installed. One of the main parameters for higher resolution is the local divergence of the incident beam: it is mainly governed by the characteristic emission of the storage ring (see page 18) it is however lower than the intrinsic reflection width of the crystal. The reflected light can be recorded on photographic plates or even by a video-system owing to the high intensity of the beam. In this latter case the geometrical resolution is not as good as on usual nuclear photographic plates; however it is used to do kinetic studies like phase transitions, twinning or plastic deformation. The size of the beam at a topographic station is usually about 1 cm high and a few centimeters wide, which needs a remote position of the experiment with respect to the storage ring output.

1.2. Observation of Phase Transitions in quartz. Quartz undergoes the well-known α-β phase transition at 846 K; moreover α quartz presents frequently Dauphiné twin (180° about c axis). The different phases, α and β (respectively 32 and 622 symmetry), and the twinned regions α_1 and α_2 satisfy simultaneously the Bragg condition for all lattice planes. However, for some reflections the structure factors differ for the α_1, α_2 and β phases. By taking X-ray topographs of e.g. $30\bar{3}1$ reflection, α and β phases (at the transition temperature) or α_1 and α_2 regions (at lower temperatures) can be identified using intensity differences (Lang 1965).

A z-cut plate of quartz ($10 \times 10 \times 1$ mm) was mounted on the sample holder of the heating unit designed by Gastaldi et al. (1982) and studied by using the white-beam technique. After indexing the Laue pattern, several temperature cycles through the transition temperature were followed by adjusting the TV camera on various diffraction spots. It was thus possible to follow continuously the features associated with the transition during the heating or the cooling of the sample by direct viewing on the TV monitor and storing on a video tape recorder.

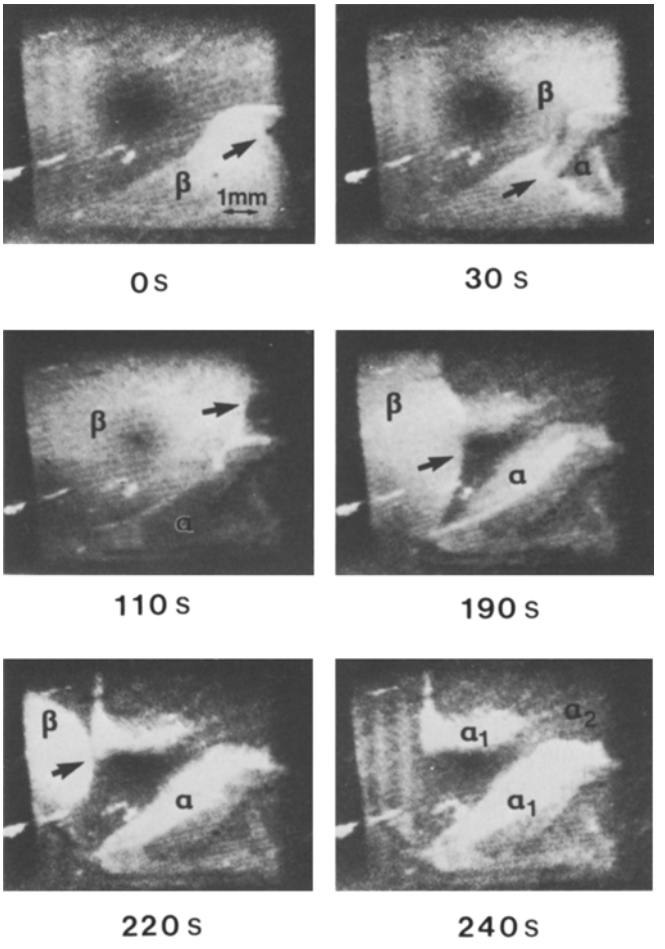

Fig. 21. Synchrotron Radiation X-ray topographs. $30\bar{3}1$ reflection. Inverted contrast. Mounting of the different stages of the development of the α phase (α_1 and α_2 domains) on cooling the sample through the transition temperature. The arrow indicates the position of the front between α and β phases. Below each photograph obtained from the video tape we have noted the time in seconds

Such an evolution is illustrated in Figure 21: the phase (α_1 and α_2 domains) develops on cooling the sample through the transition temperature. Below each photograph from video tape, representing a $30\bar{3}1$ diffraction spot topograph, the time is indicated in seconds. The progression of the α-β boundary can thus be followed and the velocity of progression measured as well as the influence on this latter of the various lattice defects. Such an example illustrates the usefulness of synchrotron radiation for obtaining original data on kinetic phenomena concerning structural modifications: together with phase transition studies, other types of topographic studies can also be performed, concerning e.g. plastic deformation of natural monocrystal.

2. Monochromatic Topography

2.1. Experimental. Among the different topographic techniques, two-crystal spectrometers have been frequently used

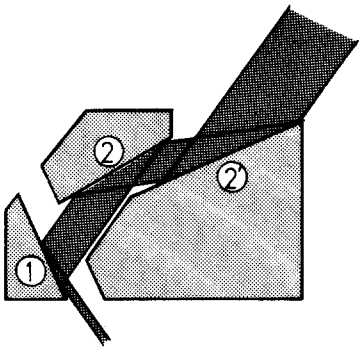

Fig. 22. Raypath in the multiple reflections monochromator.

to reveal and measure minute distortion in crystals. Generally a reference crystal both perfect and identical to the investigated sample is required and such condition prevents double-crystal studies on numerous materials for which no perfect crystals exist: this is a serious limitation for mineralogical applications. In order to overcome this difficulty two-axis spectrometers have been designed which use on the first axis high-resolution monochromators. These latter are based on the multiple reflection system (Petroff et al. 1980) which implies three successive reflections (Fig. 22). The reflections 1 and 2 define the output wavelength and the spectral resolution, and the reflections 2 and 2′ define the angular divergence of the exit beam. It is then possible to extract from the incident beam an extended plane wave with a spectral resolution $\Delta\lambda/\lambda$ better than 10^{-5}. On the second axis of the spectrometer the samples are adjusted at the chosen reflection.

With this highly monochromatized beam it is possible to record series of reflection topographs taken at different positions on the rocking curve of the crystal. Very minute defects can thus be evidenced such as rotation or dilatation of lattice planes. The high intensity of the synchrotron radiation allows one to get a greater quantity of data which is primordial when one considers the exploration of the rocking curve for various rotations of the crystal in a plane.

2.2. Local Variations on Spacing and Orientation of Lattice Planes in Hydrothermal Synthetic Quartz. Accurate lattice distortion measurements were performed on Y-cut and Z-cut plates of different quartz monocrystals, placed on the second axis of the monochromator. Four reflection profiles were obtained, corresponding to four azimuthal positions of the sample recorded at 0°, 180°, 90° and 270°, for different regularly-spaced positions, about 10 on each profile. Analysing these data lead to the $\Delta d/d$ and $\Delta\phi$ values, respectively the variation of the lattice parameter (corresponding to the spacing between planes parallel to the sample surface) and the rotation of the various zones vs a reference zone (Zarka and Liu Lin 1983). This latter is usually chosen as the best one.

The different studies have shown that the interplanar spacing d for (010) (Y-cut plate) or (001) (Z-cut plate) varies by following the different growth sector in the range $0 < \Delta d/d < 3.10^{-5}$. Such an example is illustrated in Figure 23 concerning a Y-cut plate in a synthetic quartz. In Figure 23a is represented the rocking curve obtained for the 040 reflection. The Bragg angle is 35°6 for the $\lambda = 1.2378$ Å radiation delivered by the monochromator. In this case the estimated width of the rocking curve is about 1.3″ for a perfect crystal; due to the different zones present in the crystal, the actual rocking curve is only 2.15″ wide. Figures 23b and c represent the two reflections topographs obtained for positions 22 and 24 on the rocking curve. We may point out that the X, Z, $\bar{Z}$ growth sectors are out of reflection in Figure 23c. In Figure 23b the X, Z, $\bar{Z}$ sectors are clearly visible while $\bar{X}$ and S sectors are quite out of contrast.

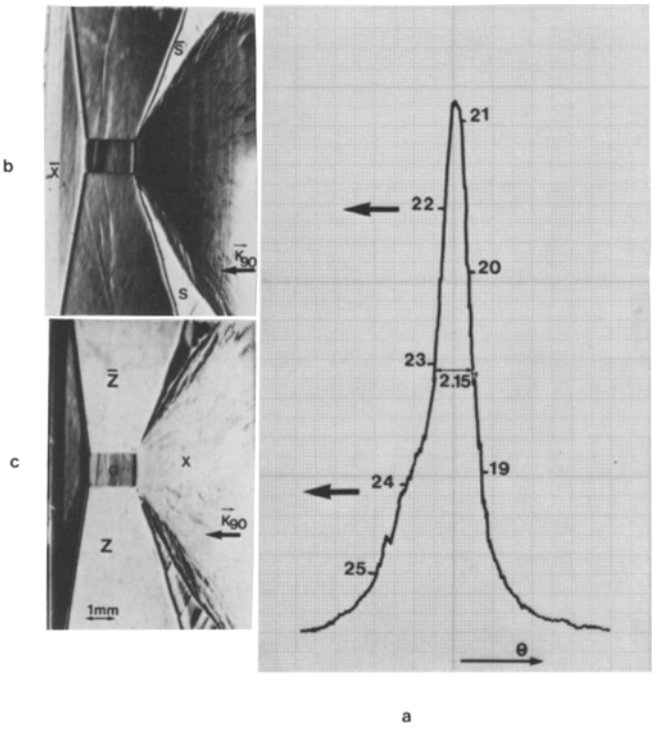

Fig. 23. (**a**) Reflection profile obtained for the 040 reflection of a Y-cut sample. (**b**) Plane wave topograph corresponding to the position 22 on the reflection profile. Note that the S and a part of $\bar{X}$ sectors are out of contrast. (**c**) Plane wave topograph corresponding to the position 24 on the reflection profile. The X, Z and $\bar{Z}$ growth sectors are out of contrast

The analysis of the 4 series of topographs corresponding to the 4 azimuths has shown that the most dilated zones are the S and $\bar{X}$ zones, where $\Delta d/d$ is about 2 to 3.10^{-5} in regard to the Z zones. Correlatively the calculation of the rotations of the lattice planes have shown that they are most effective around the $\vec{X}$ axis (Zarka et al. 1983) in the X and S regions (about 2′). Such a detailed analysis is a potentially powerful tool for a better understanding of growth conditions of the crystal.

Conclusion

Synchrotron radiation offers new prospects in Mineralogy owing to its specific unique properties, namely high intensity, white beam character and geometrical definition. We have presented in this paper some of the methods which take advantage of these properties and are in course of application to minerals and related compounds. We can summarize two kinds of progress which have been made:

– Observation of kinetics of phase transition and transformation processes, by using X-ray diffraction under high T, high P conditions, small-angle scattering and white beam topography. In this latter case some extension is also expected to the plastic deformation processes.

– Structural and chemical information given by X-ray absorption spectroscopy and microanalysis, which takes advantage of the white light character of this radiation. In particular EXAFS appears as one of the most powerful techniques – in spite of its intrinsic limitations – for studying disordered systems and local order in crystals.

Progress is expected in two distinct ways: kinetic studies, owing to the development of real-time acquisition of data for most techniques, and studies of diluted systems because of the improvement of sensitivity with techniques such as X-ray fluorescence analysis or fluorescence detection of EXAFS. Taking also into account the possibilities of the existing techniques and the fact that the number of storage rings is increasing around the world with entirely dedicated high power machines, it is to be expected in the near future a strong increase of the use of synchrotron radiation in Mineralogy and related fields.

Acknowledgements. We used the data of various teams developing mineralogical studies with synchrotron radiation:
– for X-ray absorption spectroscopy, G.E. Brown and G.D. Waychunas at Stanford Synchrotron Radiation Laboratory (SSRL), D. Bonnin, A. Decarreau and A. Manceau at Laboratoire pour l'Utilisation du Rayonnement Electromagnétique (L.U.R.E.);
– for diffraction studies under high P–high T conditions, M.D. Furnish, I.C. Huang and P. Shen at Cornell High Energy Synchrotron Source (CHESS);
– for small-angle X-ray scattering, J.Y. Bottero at L.U.R.E.;
– for X-ray microanalysis, E. Bigler, F. Polack, S. Lowenthal, A. Martin and M. Riviere at L.U.R.E.

References

Arrhenius G, Cheung K, Crane S, Fisk M, Frazer I, Korkisch J, Mellin T, Nakao S, Tsai A, Wolf G (1979) Counterions in marine manganates. In "La Genèse des nodules de manganèse". Colloq Int CNRS, C Lalou Ed, 333–356

Belli M, Scafati A, Bianconi A, Mobilio S, Palladino L, Reale A, Burattini E (1980) X-ray absorption near edge structures (XANES) in simple and complex Mn compounds. Solid State Commun 35:355–361

Besnus Y, Fusil C, Janot C, Pinta M, Sifferman G (1975) Characteristics of some weathering products of chromitic ultrabasic rocks in Bahia State, Brasil: nontronites, chlorites and chromiferous talc. Proc Int Clay Conf, 27–34

Bianconi A, Dell'Aricia M, Durham PU, Pendry JB (1981) Multiscattering resonance and structural effects in the X-ray absorption edge of FeII and FeIII hexacyanide complexes. SERC, Daresbury, Report 60 ABT, 16 p

Bianconi A, Giovanelli A, Davoli I, Stizza S, Palladino L, Gzowski O, Murawski (1982) XANES (X-ray Absorption Near Edge Structure) of V in vanadium-iron phosphate glasses. Solid State Commun 42:547–551

Bigler E (1982) Microanalyse sélective en rayons X au voisinage d'un seuil d'absorption: Comment obtenir des résultats quantitatifs grand champ par microscopie de contact X. Thèse 3ème cycle, Université Paris Sud-Orsay (n° 3154)

Bigler E, Polack F, Lowenthal S (1982) X-ray microanalysis near an absorption edge using synchrotron radiation: how to obtain quantitative results. Opt Commun 41:6

Bonnin D, Muller S, Calas G (1982) Le fer dans les kaolins. Étude par spectrométries RPE, Mössbauer, EXAFS. Bull Minéral 105:467–475

Bonnin G, Calas G, Suquet H, Pezerat H (1984) Site occupancy of Fe^{3+} in Garfield nontronite: a spectroscopic study. Submitted to Phys Chem Minerals

Bottero JY, Cases JM, Fiessinger F, Pirier JE (1980) Investigation of the hydrolysis of aqueous solutions of aluminium chloride. 1: Study of the species by NMR and potentiometry. J Phys Chem 84:2933

Bottero JY, Tchoubar D, Cases JM, Fiessinger F (1982) Id. 2: Nature and structure by small angle X-ray scattering. J Phys Chem 86:3667

Brown GE, Keefer KD, Fenn PM (1979) Extended X-ray absorption fine structure (EXAFS) study of iron-bearing silicate glasses. Abstr Geol Soc Amer 10:373

Brown GE, Dikmen FD, Waychunas GA (1983) Total electron yield K-XANES and EXAFS investigation of aluminium in amorphous and crystalline aluminosilicates. SSRL Report 83/01, 146–147

Buras B, Staun-Olsen J, Gerward L, Will G, Hinze E (1977) X-ray energy dispersive diffractometry using synchrotron radiation. J Appl Crystallogr 10:431–438

Calas G, Petiau J (1983a) Structure of oxide glasses: spectroscopic studies of local order and crystallochemistry. Geochemical implications. Bull Minéral 106:33–35

Calas G, Petiau J (1983b) Coordination of iron in oxide glasses through high-resolution K-edge spectra: informations from the pre-edge. Solid State Commun 48:625–629

Calas G, Petiau J (1984) X-ray absorption spectra at the K-edges of 3d transition elements in minerals and reference compounds. Submitted to Bull Minéral

Calas G, Levitz P, Petiau J, Bondot P, Loupias G (1980) Étude de l'ordre local autour du fer dans des verres silicatés naturels et synthétiques à l'aide de la spectrométrie d'absorption X. Rev Phys Appl 15:1161–1167

Cosslet VE, Nixon WC (1960) X-ray absorption microanalysis. In "x-ray microscopy". Cambridge Univ Press

Cotton FA, Hanson HP (1956) Soft X-ray absorption edges of metal ions in complexes. II: Cu K edge in some cupric complexes. J Chem Phys 25:619–623

Cox AD, McMillan PW (1981) An EXAFS study of the structure of lithium germanate glasses. J Non Crystallogr Solids 44:257–264

Decarreau A (1982) Étude expérimentale de la cristallogénèse des smectites. Mesures des coefficients de partage smectities trioctaédriques – solutions aqueuses pour les métaux M^{2+} de la première série de transition. Thesis, Univ. Paris-Sud – Orsay, unpublished

Eisenberger P, Brown GS (1979) The study of disordered systems by EXAFS: limitations. Solid State Commun 29:481–484

Furnish MD, Bassett WA (1983) Investigation of the mechanism of the olivin-spinel phase transition by synchrotron radiation. J Geophys Res 88:10333–10342

Gastaldi J, Jourdan, Marzo P, Allasia C, Jullien JN (1982) Ultra-high vacuum heating camera for "in situ" synchrotron radiation X-ray topographic studies. J Appl Crystallogr 15:391–395

Glatter O, Kratky O (1982) Small-angle X-ray scattering. Academic Press New York London

Greaves GN, Durham PJ, Diakun G, Quinn P (1981a) Near-edge X-ray absorption spectra for metallic Cu and Mn. Nature 294:139–142

Greaves CN, Fontaine A, Lagarde P, Raoux D, Gurman SJ (1981b) Local structure of silicate glasses. Nature 293:611–616

Guinier A, Fournet G (1955) Small-angle scattering of X-rays. John Wiley, New York

Hahn JE, Scott RA, Hodgson KO, Doniach S, Desjardins SR, Solomon EI (1982) Observation of an electric dipole transition in the X-ray absorption spectrum of a Cu(II) complex. Chem Phys Lett 88:595–598

Hannoyer B, Durr J, Calas G, Petiau J, Lenglet (1982) Caractérisation d'oxydes de cuivre par spectrométrie d'absorption X. Mat Res Bull 17:435–442

Hart M (1975) Synchrotron radiation – Its applications to high speed, high resolution X-ray diffraction topography. J Appl Crystallogr 8:436–444

Hasnain SS, Hukins DWL (1981) Some minerals and rebated calcium phosphates in "EXAFS for inorganic systems". Garner and Hasmain Eds, SERC Daresbury, 112–114

Hayes TM, Boyce JB (1982) Extended X-ray Absorption Fine Structure Spectroscopy. Solid State Phys 37:173–365 (Acad Press)

Herres N, Lang AR (1983) X-ray topography of natural Beryl using synchrotron and conventional sources. J Appl Crystallogr 16:47–56

Huang HW, Liu W, Buchanan JA (1983) Time resolved extended X-ray absorption fine structure. Nucl Instrum Methods 205:375–377

Ingalls R, Garcia GA, Stern FA (1978) X-ray absorption at high pressure. Phys Rev Lett 40:334–336

Kirz J (1980) Mapping the distribution of particular atomic species. Ann NY Acad Sci 342:273

Kunz C (ed) (1979) Synchrotron radiation-Techniques and applications. Topics in Current Physics, Springer, Berlin Heidelberg New York

Kutzler FW, Natoli CR, Misemer DK, Doniach S, Hodgson KO (1980) Use of one-electron theory for the interpretation of near edge structure in K-shell X-ray absorption spectra of transition metal complexes. J Chem Phys 73:3274–3288

Lagarde P, Fontaine A, Raoux D, Sadoc A, Migliardo P (1980) EXAFS studies of strong electrolytic solutions. J Chem Phys 72:3061–3069

Lang AR (1965) Mapping Dauphiné and Brazil twins in quartz by X-ray topography. Appl Phys Lett 7:168–170

Lang AR, Makepence APW, Moure M, Machado WG (1983) The variation of X-ray diffraction contrast with wavelength: a study with synchrotron radiation. J Appl Crystallogr 16:113–125

Lapeyre C, Petiau J, Calas G, Gauthier F, Gombert J (1983) Ordre local autour du germanium dans les verres du système $SiO_2-GeO_2-BeO_2-Na_2O$: étude par spectrométrie d'absorption X. Bull Minéral 106:77–85

Lee PA, Citrin PH, Eisenberger P, Kincaid BM (1981) Extended X-ray fine structure – its strengths and limitations as a structural tool. Rev Modern Phys 53:769–805

Lemonnier M, Fourme R, Rousseaux F, Kahn R (1978) X-ray curved crystal monochromator system at the storage ring DCI. Nucl Instrum Methods 153:173–177

Lenglet M, Le Calonnec D, Durr J, Hannoyer B, Calas G, Petiau J, Jeannot F (1983) Contribution de la spectrométrie X à l'étude d'oxydes de fer à valence mixte. Analyse de la structure fine du seuil d'absorption K. Mat Res Bull 18:935–944

Manceau A, Calas G (1984) Heterogeneous distribution of nickel in hydrous silicates from New Caledonian ore deposits. Submitted to Am Mineral

Petiau J, Calas G (1982) Local structure about some transition elements in oxide glasses using X-ray absorption spectroscopy. 5th Int Conf on "Physics of Non-crystalline Solids" J Phys C9:47–50

Petiau J, Calas G, Bondot P, Lapeyre C, Levitz P, Loupias G (1981) EXAFS and near-edge structures of some transitions elements and germanium in silicate glasses. In "EXAFS for Inorganic Systems", NERC, 127–129

Petroff JF, Sauvage M, Riglet P, Hashizume H (1980) Synchrotron radiation plane-wave topography. I. – Application to misfit dislocation imaging in III–V heterojunctions. Philos Mag 42:319–338

Phizackerley RP, Rek ZU, Stephenson GB, Conradson SD, Hodgson KO, Matsushita T, Oyanagi H (1983) An energy-dispersive spectrometer for the rapid measurement of X-ray absorption spectra using synchrotron radiation. J Appl Crystallogr 16:220–232

Poirier JP (1981) The kinetics of olivine-spinel transition. Phys Earth Planet Interiors 226:179–187

Polack F, Lowenthal S, Petroff Y, Farge Y (1978) Selective X-ray absorption microanalysis with synchrotron radiation. Nucl Instrum Methods 152:289

Pons CH, Rousseaux F, Tchoubar D (1981) Utilisation du rayonnement synchrotron en diffusion aux petits angles pour l'étude du gonflement des smectites. Partie I: Etude du système eau-montmorillonite Na en fonction de la température. Clay Miner 16:23–42

Pons CH, Rousseaux F, Tchoubar D (1982) Id. Partie 2: Etude de différents systèmes eau-smectites en fonction de la température. Clay Miner 17:327–328

Raoux D, Petiau J, Bondot P, Calas G, Fontaine A, Lagarde P, Levitz P, Loupias G Sadoc A (1980) L'EXAFS appliqué aux déterminations structurales de milieux désordonnées. Rev Phys Appl 15:1079–1094

Regnard JR, Chavez-Rivas F, Chappert J (1981) Study of the oxidation states and magnetic properties of iron in volcanic glasses: Lipari and Teotihuacan obsidians. Bull Minéral 104/204–210

Sandstrom DR (1982) Studies of metal-ion complexes in aqueous solutions by EXAFS and XANES spectroscopy. Trans Amer Geophys Union, EOS 63:1129

Sauvage M, Petroff JF (1980) Application of synchrotron radiation to X-ray topography. In "Synchrotron Radiation Research", H Winick, S Doniach (eds) Plenum Press, New York, 607–638

Scandale E, Zarka A (1982) Sur l'origine des canaux dans les cristaux. J Appl Crystall 15:417–422

Skelton EF, Qadri SB, Webb AW, Lee CW, Krikland JP (1983) Improved system for energy-dispersive X-ray diffraction with synchrotron radiation. Rev Sci Instrum 54:403–409

Srivastava UC, Nigam HL (1973) X-ray absorption edge spectrometry (XAES) as applied to coordination chemistry. Coord Chem Rev 9:275–310

Steinberg M, Polack F., Riviere M., Martin A (1979) Utilisation du rayonnement synchrotron pour la localisation d'éléments à l'échelle de la lame mince dans diverses concrétions polymétalliques. In «La genèse des nodules de manganèse», Colloq Int CNRS, C Lalou Ed, 357

Steinberg M, Bigler E, Tlig S, Bonnot-Courtois C, Desprairies A, Lallier-Verges E, Riviere A, Marcoux J (1983) Comparaison des caractéristiques texturales et géochimiques de quelques concrétions ferro-manganésifères récentes et fossiles. Bull Soc Géol Fr, to be published

Stern EA, Sayers DE, Lytle FW (1975) Extended X-ray absorption fine-structure technique. III. – Determination of physical parameters. Phys Rev B11:4836–4845

Tchoubar D, Rousseaux F, Pons CH, Lemonnier M (1978) Small-angle scattering setting at L.U.R.E.: description and results Nucl Instrum Methods 152:301–305

Teo BK, Lee PA (1979) Ab-initio calculations of amplitude and phase functions for Extended X-ray Absorption Fine Structure (EXAFS) Spectroscopy. J Am Chem Soc 101:2815

Tuomi T, Naukkarinen K, Rabe P (1974) Use of synchrotron radiation in X-ray topography. Phys Status Solidi A25:93–106

Vaughan DJ (1978) The interpretation and prediction of the properties of opaque minerals from crystal chemical models. Bull Minéral 101:484–497

Waychunas GA, Apted MJ, Brown GE Jr (1983) X-ray K-edge absorption spectra of Fe minerals and model compounds. Near-edge structure. Phys Chem Minerals 10:1–9

Will G (1981) Energiedispersion and Synchrotronstrahlung: eine neue Methode und eine neue Strahlenquelle für die Röntgenbeugung. Fortschr Mineral 59:31–94

Winick H (1980) Properties of synchrotron radiation. In "Synchrotron Radiation Research", H Winick, S Doniach (eds), Plenum Press, New York

Yakel HL (1980) Determination of the cation site-occupation parameter in a cobalt ferrite from synchrotron radiation diffraction data. J Phys Chem Solids 41:1097–1104

Zarka A, Liu Lin (1983) Study of local variation in spacing and orientation in a Z-cut plate of synthetic quartz by X-ray topography. J Crystallogr Growth, 61:397–405

Zarka A, Liu Lin, Sauvage M (1983) Etude des variations locales d'espacement et d'orientation des plans réticulaires dans des quartz de synthèse. J Cryst Growth 62:409–424

Received March 21, 1983